

# A Kalman Filter to Improve Measurements of Wind from NSF/NCAR Research Aircraft

William A. Cooper

**DRAFT** 3/6/2017  
(title page to be replaced by NCAR library template)

National Center for Atmospheric Research  
Earth Observing Laboratory  
Research Aviation Facility



# Contents

<b>1</b>	<b>Introduction</b>	<b>1</b>
1.1	Overview . . . . .	1
1.2	Brief summary of the Kalman filter . . . . .	3
<b>2</b>	<b>The derivative of the state vector</b>	<b>5</b>
2.1	The procedure to be used . . . . .	5
2.2	Components of the derivative array . . . . .	6
2.3	Tests of the derivatives . . . . .	7
2.4	Mechanization using the derivatives . . . . .	11
<b>3</b>	<b>Ancillary topics</b>	<b>15</b>
3.1	A new variable for rate of climb . . . . .	15
3.2	Retrieving IRU measurements by differentiation . . . . .	17
3.3	Simpler algorithms . . . . .	18
3.4	Angle of attack . . . . .	24
<b>4</b>	<b>The Kalman filter</b>	<b>26</b>
4.1	The algorithm used . . . . .	26
4.2	Detecting the error in heading . . . . .	29
4.3	Smoothing the errors in pitch and roll . . . . .	32
4.4	Results . . . . .	33
<b>5</b>	<b>New variables for wind</b>	<b>42</b>
5.1	Calculating the wind . . . . .	42
5.2	Adding the new variables to the netCDF file . . . . .	46
<b>6</b>	<b>Summary and conclusions</b>	<b>51</b>
<b>A</b>	<b>Appendix: Reproducibility</b>	<b>52</b>
<b>References</b>		<b>53</b>
<b>Variable Names and Acronyms</b>		<b>54</b>
<b>Index</b>		<b>55</b>

## List of Figures

1	Comparison of IRU-measured accelerations to the accelerations determined by differentiating the velocity components measured by the GPS receiver. . . . .	10
2	Comparison of INS-provided and integration-derived attitude angles. . . . .	12
3	Comparison of INS-provided and integration-derived components of the aircraft velocity. . . . .	13
4	Comparison of a new variable representing rate of climb to the corresponding GPS-based measurement and the INS-provided measurement. . . . .	16
5	Comparison of measured body rotation rates and those determined by differentiating the attitude angles, for a flight segment with various maneuvers. . . . .	19
6	Comparison of the Kalman filter, GPS, and INS values for latitude, longitude and altitude, with corrections from the Kalman filter also shown. . . . .	34
7	Comparison of the Kalman filter, GPS, and INS values for aircraft-velocity components, with corrections from the Kalman filter also shown. . . . .	36
8	Errors in pitch and roll after transformation to the l-frame with a filtered result and bands of uncertainty. . . . .	37
9	Errors in pitch and roll that result from transforming the filtered result in the previous figure back from the l-frame to the a-frame. . . . .	38
10	The flight track of about 7 h duration for DEEPWAVE flight 16, 4 July 2012. .	39
11	Heading error estimated from Eqn. 15 (top), and the results from the Kalman filter and a simplified estimate of the error in heading (bottom). . . . .	40
12	Variance spectra for the rate-of-climb measurements from the GPS receiver and the integrated INS-provided acceleration. . . . .	43
13	Variance spectra for two measurements of the vertical wind, WIKF as adjusted by the Kalman filter and WIC from conventional data processing. . . . .	44
14	Vertical wind calculated using the results from the Kalman filter, compared to the original calculation before Kalman-filter correction. . . . .	45
15	Differences between the conventional measurements of horizontal wind and the results from the Kalman filter. . . . .	47
16	Variance spectra for the standard measurements of the longitudinal and lateral components of the horizontal wind and for the corresponding results after correction by the Kalman filter. . . . .	48

## List of Tables

1	Results of regression fitting the $l$ -frame acceleration as a function of the derivative of the variable listed in the “fit” column. The coefficients represent, for example, $\dot{v}_e \sim c_0 + c_1 a_e^l$ where $a_e^l$ is the eastward component of acceleration after transformation to the $l$ -frame. The residual standard deviation is tabulated as $\sigma$ , and the square of the correlation coefficient is $R^2$ . . . . .	8
2	Results like those in the preceding table but for accelerations in the $a$ -frame. . .	8
3	Comparison of the rate of change in heading ( $\psi$ ) to the rate of change in the direction of the acceleration vector determined from differentiation of GPS-based velocity components ( $\psi^*$ ). All units are [ ${}^\circ\text{s}^{-1}$ ]. The listed standard deviations are those estimated for the mean measurement. . . . .	11

## **Prefix and Abstract**

To improve the measurements of wind made from NSF/NCAR aircraft, a Kalman filter is developed and applied to archived data files from research projects. The filter is an error-state Kalman filter, and the emphasis is on improving the measurements of pitch and heading because they are usually the dominating source of uncertainty in measured wind. The NSF/NCAR Gulfstream V research aircraft is emphasized in the development, but the filter as developed can be applied to data from other present and past NCAR aircraft as well. So that the resulting filter can be applied in cases where the primary measurements from the inertial reference system were not recorded in the data file, a method is developed for retrieving those measurements by differentiating the recorded variables representing attitude angles and aircraft-velocity components. In addition, some new algorithms are introduced for estimating the rate of climb of the aircraft from the measured accelerations and for estimating the angle of attack from pressure measurements made at ports on the radome. In addition, simplified methods for estimating the errors in pitch and heading without the full complexity and processing requirements of the Kalman filter are documented. The result is that standard uncertainties in pitch and heading are reduced to about  $0.01^\circ$ , so that they no longer dominate the uncertainty in the wind measurements. Some examples illustrate the effects of the Kalman filter on measured wind and on variance spectra. The processing technique is incorporated into an R script that can add the improved variables to a standard netCDF data archive so that they can be made available for community use. Documents that are accessible via links in this technical document provide information on the workflow that generated the document, the details of the processing algorithms, and instructions for use and modification of the processing script.

## Acknowledgments

The research aircraft discussed in this technical note, the NSF/NCAR Gulfstream V often called "HIAPER", was the result of an extensive effort both within and outside of NCAR, and at the National Science Foundation. Chris Webster's development and maintenance of the software used for data processing was a very important contribution to this effort. The technical staff of the NCAR Earth Observing Laboratory were involved in all stages of the development and operation of this research platform, and the project management staff, operations staff, and computing and data management groups of that Laboratory conducted the projects that produced the data used in this document. Without all these contributions, the measurements characterized in this document would not have been available to the community. NCAR is sponsored by the National Science Foundation (NSF), and the NSF also supported the experiments that collected the data used in this technical note.

The data used in the examples presented are from the DEEPWAVE project (Deep Propagating Gravity Wave Experiment over New Zealand), described at [https://www.eol.ucar.edu/field\\_projects/deepwave](https://www.eol.ucar.edu/field_projects/deepwave). [NEED A DATA CITATION HERE] Measurements were collected by the DEEPWAVE experiment team, and flight operations and data acquisition and processing were performed by the Research Aviation Facility, Earth Observing Laboratory, National Center for Atmospheric Research (NCAR). The analyses reported here were mostly performed using R Core Team [2016], with RStudio RStudio [2009] and knitr Xie [2013, 2014]. Substantial use also was made of the ggplot2 package Wickham [2009] for R. The code used for the Kalman filter relies on the Jacobian function in the R package “numDeriv” version 2016.8-1; cf. Gilbert and Varadhan [2016].



# 1 Introduction

## 1.1 Overview

A recent technical note ([Cooper et al. \[2016\]](#)) discussed the uncertainty associated with measurements of wind from the NSF/NCAR Gulfstream V research aircraft, hereafter called the GV. The aircraft is owned by the National Science Foundation (NSF) and operated by the Research Aviation Facility (RAF), Earth Observing Laboratory (EOL), National Center for Atmospheric Research (NCAR). The components and algorithms that comprise the wind-measuring system on the GV were documented in that reference, so that information will not be repeated here. The central content of that technical note was a detailed analysis of uncertainty for the wind measurements. The standard uncertainty was estimated to be about  $0.1 \text{ m s}^{-1}$  for vertical wind and  $0.4 \text{ m s}^{-1}$  for each component of the horizontal wind. These estimates were based on the analyzed performance of the inertial navigation system, and are lower than would be expected from direct specifications for that system. The largest contributions to uncertainty were associated with the measurements of pitch and heading, for respectively the vertical and horizontal wind components. Improvement in the measurements of these attitude angles therefore is the indicated step toward improved measurements of wind.

Two approaches are taken in the present technical note to improve the key measurements. The first uses a simplified analysis of the strong coupling represented by the Schuler oscillation to evaluate errors in pitch and combines this with a related analysis to find the correction in heading. The second implements a full error-state Kalman filter to produce adjusted measurements of the attitude angles and also the ground-speed components and rate-of-climb of the aircraft. The agreement between these two methods then supports the validity of each, while the first provides a much simpler method for determining the corrections.

This introduction will discuss the steps involved in using an error-state Kalman filter to update measurements from the inertial systems on the aircraft (which do not have internal Kalman filters) using reference measurements from a Global Positioning System (GPS) receiver. The measurements from the GPS receiver are very good for aircraft position and velocity, so the Kalman filter adds little to these measurements. The primary value of the Kalman filter presented here is that it improves the measurements of pitch and heading.

Section 2 next will develop expressions for the derivatives of a nine-component “state vector” of measurements from the inertial navigation system (INS), representing aircraft position, velocity, and attitude, and will show that these derivatives provide a reasonable basis for mechanization, i.e., calculating the history of the state vector of the aircraft from the basic measurements provided by the inertial reference unit (IRU).<sup>1</sup> Those basic measurements are the vector rotation rate and vector acceleration of the aircraft in an inertial frame, so the test of the calculated derivatives is that the results for the sequence of state vectors should be in reasonable agreement with the values provided by the INS. The importance of this step is that the validated state-vector derivative then will be used in implementation of the error-state Kalman filter.

---

<sup>1</sup>In this document, IRU will refer to the portion of the instrument that produces the basic measurements of body acceleration and body rotation rate, while INS will refer to the full system that uses those basic measurements to propagate the position, velocity, and attitude angles of the aircraft forward in time from an initial state determined during alignment of the instrument.

Section 3 is a diversion from the main development of this technical note. It discussed several ancillary topics:

- i. a new variable representing the rate of climb of the aircraft that is an improvement over the measurement provided by the INS;
- ii. a method for finding the IRU-provided measurements of rotation and acceleration by differentiating the recorded attitude angles;
- iii. simplified algorithms for finding the errors in pitch and heading; and
- iv. a revised empirical representation of angle of attack.

The first is useful because the INS internally updates the variable representing the vertical speed of the aircraft by comparison to the pressure altitude, while the measurement of wind needs a variable representing the rate of change in geometric altitude. The second topic is needed because, for many of the early research projects using the GV, the body rotation rates and body accelerations were not recorded, yet they are needed by the Kalman filter. Reconstructing them makes it possible to process those older projects or to process from the standard data archives, which normally do not include the body rotations even if they were present in the original recorded file. The third topic provides a complementary approach to finding the same errors in attitude angles that the Kalman filter will produce. It will provide a useful test of the results from that filter. Finally, Sect. 3.4 extends the discussion of sensitivity coefficients contained in [Cooper et al. \[2016\]](#) by presenting a new empirical representation that has advantages over the method used previously. Improved pitch measurements lead to improved coefficients used in this empirical representation, so that is an added benefit of the Kalman filter. These will find important uses in the implementation of the Kalman filter or the new calculation of wind that is based on the corrections it provides.

Section 4 then discusses the details of the Kalman filter. A script based on the R programming language has been developed to calculate the estimated errors from the Kalman filter, apply the indicated corrections to the measured state vector, and add those new variables to the standard netCDF data file. This section includes discussion of the aspects of that code that represent the Kalman filter. The results are shown and compared to reference results and to the alternate methods of determining the pitch and heading corrections as discussed in Sect. 3.

Section 5 shows examples of the measurements of wind based on the corrected state vector. The conclusion of this section and the closing section summarize the value of the Kalman filter. At the end, there is also a list of netCDF variable names referred to in the text, with definitions, and an index.

A goal of this project has been to make this work internally documented and reproducible, as discussed in the Appendix. The program that produces this document (via  $\text{\LaTeX}$ ), named `KalmanFilterTechNote.Rnw`, also performs all the calculations, generates the quoted results and figures (with a few exceptions), and produces the new archive file, so that program file contains everything needed to reproduce this work. Subsets of the data files are also preserved and archived. Another document called the workflow document (`KalmanFilterWorkflow.pdf`)

accompanies this technical note and the generating program file. It serves several purposes, primarily to elaborate upon the material in the present document. Some of the derivations are justified in more detail, and instructions are provided for running the R script to add the corrected variables to a netCDF file. Some details of how that modification of an existing file is done are included in the workflow document, and there is also some discussion of methods that were explored but abandoned in the course of this work. The workflow document should provide valuable information to anyone wanting to modify the R script or use it to process archival data files.

## 1.2 Brief summary of the Kalman filter

A Kalman filter provides a means of updating a sequence of state vectors (consisting, in the present case, of INS-provided measurements of position, velocity, and attitude angles) by comparison to an independent set of measurements (e.g., GPS-based measurements of position and velocity). The updated state vector obtained by this process consists of an appropriately weighted combination of the state vector projected forward using normal mechanization and the independent measurements from the GPS receiver. Because errors in the state vector are coupled, the update procedure can estimate errors in the attitude angles as well as in the components of the state vector that are measured directly by the GPS receiver. This correction to attitude angles is the primary reason for using a Kalman filter to improve the wind measurements.

The weighting of the projected-forward state vs. new measurements from the GPS receiver depends on estimates of the covariance matrix describing the state vector as well as estimates of the noise contaminating the measurements from the GPS receiver and the accelerations and rotation rates from the IRU. With proper weighting, the result should combine the good high-frequency response of the INS with the good long-term stability of the GPS-based measurements. The covariance matrix characterizing the state vector is updated as the filter is applied, but appropriate weighting depends on reasonable estimation of the other error terms.

The operation of the filter depends on sequential use of a set of matrices, so it is useful to define those as follows, where the variable names following the symbols are the R variable names used in the R code:

$\delta\mathbf{x}_k$  [SVE] The error-state vector at time index  $k$ . In the present case, this consists of these 15 components: estimated errors in position, aircraft velocity, aircraft attitude, IRU-measured rotation rate, and IRU-measured accelerations.

$\mathbf{T}_{k|k-1}$  [dcm] The  $15 \times 15$  state transition matrix based on the derivatives used for INS mechanization, for the change from time  $k - 1$  to time  $k$ . Then  $\delta\mathbf{x}_k = \mathbf{T}_{k|k-1}\delta\mathbf{x}_{k-1}$  where  $\mathbf{T}$  combines the unit diagonal matrix with the time step multiplied by the derivative matrix describing the state transition. As applied to the state vector, a state transition vector would involve the derivatives used for normal mechanization to advance the state vector and so would duplicate the action of the internal INS data processing. As interpreted for an error-state Kalman filter, the matrix  $\mathbf{T}$  is obtained by calculating the Jacobian of the function of the state vector that produces that

derivative vector, as a function of the error-state components; i.e.,  $T[i, j]$  is the derivative of the  $i$  component of that derivative function with respect to change in the  $j$  component.

- V [CV]** The  $15 \times 15$  covariance matrix that applies to the state vector  $\delta\mathbf{x}$ .
- K [K]** The Kalman-gain matrix representing how the error-state vector is updated using the current error state and the new GPS-based measurements.
- $\delta\mathbf{z}$  [DZ]** The 6-component error vector containing the measured differences between the INS and GPS-based measurements of position and velocity.
- H [H]** The  $15 \times 6$ -component observation matrix representing how the measured differences  $\delta\mathbf{z}$  correspond to the error-state vector.
- Q, R [Q, R]** Matrices representing respectively the noise contributions ( $15 \times 15$ ) characterizing the forward propagation of the error-state vector and the measurements from the GPS receiver ( $6 \times 6$ ).

The approach taken here will be to use the error-state vector that represents the difference between the best-estimate measurements and those originally provided by the INS. The INS integration does not need to be duplicated; the reference integration is already available. However, the Kalman filter does need the derivative vector that leads to that forward integration, so the first step in this analysis was to develop a function for the derivative vector and validate it by comparing the mechanization that uses it to the available INS-provided variables, as described in Sect. 2.4. The Jacobian of that derivative function, evaluated at current values for the state vector including measurements from the IRU, then provides the matrix **T** used in this filter. The implementation of the Kalman filter outlined here then follows in Sect. 4.

## 2 The derivative of the state vector

### 2.1 The procedure to be used

The state vector used in this section will consist of the three components of position, three components of aircraft velocity relative to the Earth, and three attitude angles (pitch, roll and heading). In later sections a different vector, the error-state vector, will be used for the Kalman filter, and in that case three components of measured rotation rate and three components of measured acceleration will be added to the state vector so that the Kalman filter can treat the possibility of error in the latter six components as well as the first nine. However, the purpose of this section is to develop expressions for the derivatives of the nine-component state vector in terms of the IRU-measured rotation rates and accelerations and to demonstrate that the calculated derivatives lead to a reasonable mechanization that approximately duplicates the original calculations from the INS. It is not necessary or expected that this mechanization will produce an exact duplicate of the INS mechanization because the INS has high-rate data and timing information not available to this new calculation. However, if the results are reasonably close to those from the INS then that provides some evidence that the derivatives being calculated are reasonably close to the correct values. These derivatives will then be used in the implementation of the Kalman filter, where the filter will adjust to compensate for any errors remaining in these derivatives.

The procedure used to produce variables corresponding to position, velocity, and attitude angles for this test is as follows:

1. Initialize a state vector  $\mathbf{x}$  having these components:
  - (a) latitude, longitude, altitude in the  $l$ -frame, the local-level reference frame that rotates with the Earth and has axes pointing east, north, and upward at the location of the aircraft; . This reference frame, also called the local-level or ENU reference frame, has axes pointing east, north, and upward at the location of the aircraft;
  - (b) east, north, and upward velocity in the  $l$ -frame
  - (c) pitch, roll, heading in the  $a$ -frame<sup>2</sup> (the reference frame of the aircraft; cf. Sect. 2.2 item 2).
2. For each time increment:
  - (a) Calculate the time derivative of the state vector. In the case of the attitude angles, this is done by calculating the derivative of the transformation matrix from the  $a$ -frame to the  $l$ -frame and then using the definition of components of that matrix to find the derivative of the attitude angles.

---

<sup>2</sup>With appropriate transformations these calculations of attitude angles can be performed in the  $l$ -frame instead, and there are some advantages because the  $l$ -frame values of errors in pitch and roll, respectively representing southward and westward tilts of the virtual inertial platform, are not mixed together when the heading changes as they are in the  $a$ -frame. This was not done in the calculations presented here.

- (b) Use that derivative vector to increment the state vector, compensating for possible wrap-around of the heading at 0 and 360 deg so that values stay within that range.
- (c) save the nine components of the state vector in a new tabulation that represents an independent mechanization of the IRU-provided measurements. These new results should then be in reasonable agreement with the INS integration.

## 2.2 Components of the derivative array

The derivatives are calculated as follows:

1. The position derivatives are determined from the components of the velocity,  $\{v_e, v_n, v_z\}$ . The changes in latitude and longitude depend on the normal and meridional radii of curvature of the Earth, respectively denoted  $R_n$  and  $R_m$ . [Noureldin et al. \[2013\]](#), pp. 47–48, provide definitions of these radii and a detailed derivation. The derivatives of latitude  $\lambda$  and longitude  $\Phi$  are then

$$\dot{\lambda} = \frac{v_n}{R_m + z} \quad (1)$$

$$\dot{\Phi} = \frac{v_e}{(R_n + z) \cos \lambda} \quad (2)$$

where  $z$  is the altitude of the aircraft, with the derivative

$$\dot{z} = v_z \quad (3)$$

where dots over quantities denote the time derivatives.

2. The velocity derivatives are determined from the measured accelerations, but the accelerations are measured in the  $a$ -frame, with axes such that the unit coordinate vectors are  $\hat{x}$  forward along the longitudinal axis of the aircraft,  $\hat{y}$  in the direction of the starboard wing, and  $\hat{z}$  along the direction determined by their cross product and generally downward. These measurements of acceleration must be transformed to the  $l$ -frame using the attitude angles for pitch, roll, and heading, denoted  $\{\theta, \phi, \psi\}$ , because the components of velocity are defined in that frame. In addition, because the accelerations are measured in an inertial frame, corrections must be made for the inertial forces that arise because the  $l$ -frame is moving relative to the Earth and so is changing orientation, and because the rotation of the Earth introduces additional Coriolis accelerations relative to an inertial frame. The coordinate transformation matrix that transforms a vector from the  $a$ -frame to the  $l$ -frame will be denoted  $\mathbf{R}_a^l$  and consists of four sequential transformations, first a rotation by  $\phi$  about the roll axis, then a rotation by  $\theta$  about the pitch axis, then a rotation by  $\psi$  about the resulting  $\hat{z}$  axis, and finally exchange of the  $\hat{x}$  and  $\hat{y}$  components and reversal of the sign of the  $\hat{z}$  component to change to the  $l$ -frame reference frame. The transformation was presented in detail by [Lenschow and Spyers-Duran \[1989\]](#), and

is also specified and developed in the workflow document that accompanies this technical note. The  $a$ -frame measurements of acceleration are transformed to the  $l$ -frame using this transformation matrix after the acceleration of gravity is added to the normal component because the IRU reports the normal component of gravity as that with the acceleration of gravity subtracted. Then the transformed accelerations are corrected for apparent forces generated by the inertial forces. [Noureddin et al. \[2013\]](#), pp. 178–179, give the equations used, and these are repeated in the workflow document.

3. Calculating the derivatives of the attitude angles is more involved. The attitude angles can be found if the transformation matrix  $\mathbf{R}_a^l$  is known by using the definitions of the components of that matrix in terms of the attitude angles. For example, the [3, 1] component of that matrix is  $-\sin \theta$ , so  $\theta = -\arcsin(R_a^l[3, 1])$ . The measured rotation rates, transformed to the  $l$ -frame, give the derivative of the transformation matrix, except that again corrections for inertial effects arising from the Earth’s rotation and the motion of the  $l$ -frame are needed. [Noureddin et al. \[2013\]](#), pp. 179–180, also provide the required correction for the derivative of the transformation matrix, as documented further in the workflow document and the code. These corrections also are discussed in more detail in Sect. 3.2.1, equations (6)–(8).

The function “STMFV” returns these derivatives, given the state vector and the measurements from the IRU. The algorithms and code are complicated enough that validation is important, so several tests are made of the results in the remainder of this section.

## 2.3 Tests of the derivatives

### 2.3.1 Validating the transformed accelerations

The components of acceleration expressed in the  $l$ -frame can be compared to the accelerations determined by differentiating either the INS-provided or the GPS-based measurements of aircraft velocity. The former is a test of the calculation; the latter is a test of the calibration of the accelerometers. The derivatives of the velocity were determined by taking differences between consecutive measurements, although it was useful to smooth the result using a Savitzky-Golay third-order polynomial spanning 11 25-Hz samples to reduce noise arising from the limited resolution of the differences.

Relative timing among the measurements can influence these results. Many of the variables have corrections applied for assumed time-lags during measurement, so in this test of accelerations those lags were first removed. Then there were additional lags apparent among variables provided by the INS, even when tagged with the same times. To determine these lags, a pitch maneuver (where the pilots induce rapid changes in pitch with associated climbs and descents during straight flight) from DEEPWAVE (“Deep Propagating Gravity Wave Experiment over New Zealand”) research flight 15, 3 July 2014, 3:16:00–3:18:00 UTC was used. Shifting among the measurements from the INS was explored to see what provided the best agreement between measured accelerations (variables BLONGA, BLATA, BNORMA) and the accelerations determined by differentiating the INS variables for aircraft velocity (VEW, VNS, VSPD) and then

<i>fit</i>	$c_0$ [m s <sup>-2</sup> ]	$c_1$	$\sigma$ [m s <sup>-2</sup> ]	$R^2$
GPS east	-0.0002	0.99914	0.01463	0.99994
GPS north	0.00025	0.99913	0.01468	0.99994
INS east	-0.00024	0.99983	0.00776	0.99998
INS north	0.00042	0.99983	0.00731	0.99999

*Table 1: Results of regression fitting the l-frame acceleration as a function of the derivative of the variable listed in the “fit” column. The coefficients represent, for example,  $\dot{v}_e \sim c_0 + c_1 a_e^l$  where  $a_e^l$  is the eastward component of acceleration after transformation to the l-frame. The residual standard deviation is tabulated as  $\sigma$ , and the square of the correlation coefficient is  $R^2$ .*

<i>Component</i>	$c_0$ [m s <sup>-2</sup> ]	$c_1$
BLONGA	0.00079	1.00121
BLATA	0.00278	1.05649
BNORMA	-0.00555	0.99957

*Table 2: Results like those in the preceding table but for accelerations in the a-frame.*

transforming the resulting accelerations to the  $a$ -frame (where the IRU measures accelerations). That transformation must include correction for inertial effects as discussed in Sect. 2.2, item 2. The standard deviation of the difference between the measured acceleration and that determined by differentiating the measured aircraft velocity was minimized if the measurements of acceleration were moved 50 ms earlier in time, the measurements of pitch and roll were shifted 20 ms later in time, and no shift was applied to the measurements of aircraft velocity. These shifts are all important only in relation to each other; the same result was obtained if the accelerations were moved earlier by 70 ms, measurements of velocity moved earlier by 20 ms, and measurements of pitch and roll left unshifted. According to the specifications for the INS, there may be lags in the times when variables are transmitted from the unit of up to about 70 ms for accelerations and attitude angles and up to 110 ms for velocity components, so these shifts are within the approximate range expected. For the purpose of comparing accelerations, the optimal shifts were applied to the measurements for this pitch maneuver.<sup>3</sup>

Table 1 shows the results of linear fits of the measured accelerations after transformation to the  $l$ -frame (with inertial corrections) to the derivatives determined by differentiation. The GPS measurements provide independent measurements of the accelerations, so the first two fits can be considered tests of the calibrations of the accelerometers as well as a test of the algorithms and code. They indicate only small offsets and near-unity slopes. The last two fits compare only INS-provided values, so they test the validity of the transformations and protect against any unknown calibration adjustments that might have been applied by the INS without affecting the reported accelerations.

<sup>3</sup>There is no assurance that these shifts will be constant.

A better direct estimate of accelerometer calibration can be obtained by transforming the  $l$ -frame accelerations determined by differentiating the GPS-based velocity to the  $a$ -frame, where they can be compared directly to the components of the measured accelerations. When this is done, the calibrations in Table 2 result from linear fits. Lateral accelerations are usually small, so the second calibration is not as reliable as the other two, but all show reasonable agreement between the calibrations in use and those indicated by these fits. Although the small adjustments have little effect, the calibrations indicated in this table will be applied to the measured accelerations in the remainder of this technical note.

Figure 1 shows a short flight segment comparing the measured accelerations and the accelerations determined by differentiating the GPS-based velocity and transforming to the  $a$ -frame. There were three maneuvers that introduced accelerations: (i) a pitch maneuver near 3:17:00 UTC where pilots varied the pitch rapidly, causing periodic accelerations normal to the aircraft; (ii) a speed run centered near 3:25:00 UTC where the airspeed was varied through the flight envelope of the GV, producing large changes in pitch and resulting resolution of the acceleration of gravity into varying contributions to the longitudinal and normal components of acceleration; and (iii) a yaw maneuver near 3:34:00 UTC where lateral accelerations were induced by rudder action. The good agreement and the near-identity calibrations tabulated above support that the accelerations are being treated properly in the calculations and also that the calibrations of the accelerometers are good.

### 2.3.2 Validating the rotation rates

Independent measurements of rotation rates are not available as they are for accelerations, so similar direct tests and calibrations are not possible. However, if the wind remains constant, a flight maneuver consisting of a circular pattern should produce a  $360^\circ$  change in heading, and the start and end points can be identified from GPS-based measurements by finding the times when the groundspeed components return to their original values. DEEPWAVE flight 15 included several circle patterns in the flight plan, including four from 3:38:00 to 3:55:00 UTC, two counterclockwise and then two clockwise. Without inertial corrections, which are very small integrated over the circles, the rate of change in heading should be  $\dot{\psi} = \text{BYAWR}/\cos\phi$  where BYAWR is the rotation rate about the yaw axis as reported by the IRU and  $\phi$  is the roll angle, so comparing this to the change in heading tests that the reported rotation rates are correct. The total heading change from 3:38:50 to 3:46:40 is  $-718.2^\circ$ , while the sum of  $\text{BYAWR}/\cos\phi$  for the same time interval is  $-720.1^\circ$ , so these agree to within 0.2%. For the two clockwise turns from 3:46:40 to 3:54:30, the corresponding sums are 720.1 and 720.6, in still better agreement. This only tests for consistency, because the INS mechanization should produce the same result as that obtained by the difference in output variables, but one significant conclusion is that the inertial corrections have only a very small net effect on the rotation rate about the heading or yaw axis.

Another test of the rotation rate about the yaw axis can be obtained by comparing  $\dot{\psi}$  in steady turns to the rate of change in the orientation of the acceleration vector determined from the GPS. In circle maneuvers, the horizontal component of the acceleration vector should rotate at a rate equal to  $\dot{\psi}$ , so this provides a test of the calibration of the rotation rate provided by the

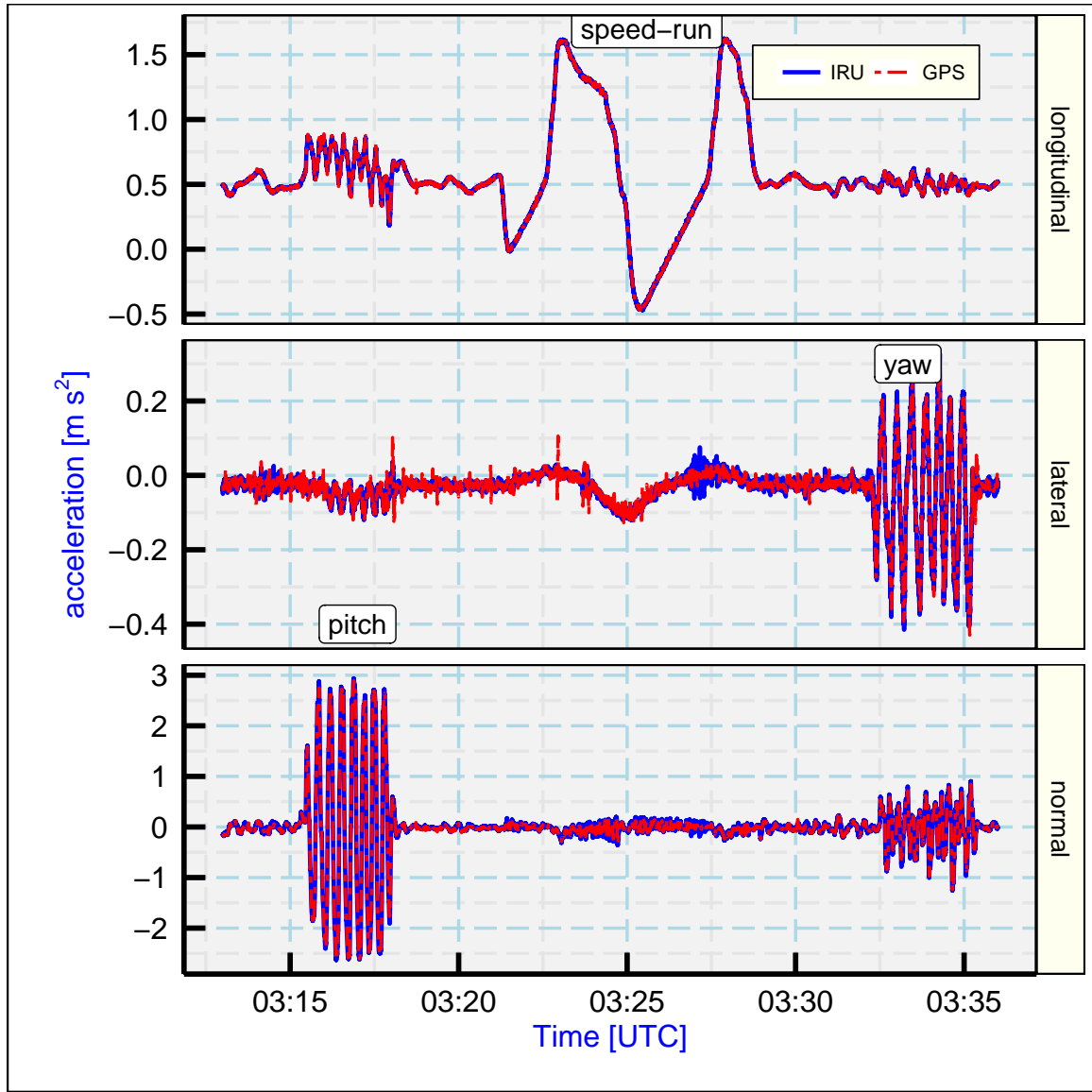


Figure 1: Comparison of measured accelerations (*BLONGA*, *BLATA*, *BNORMA*, blue lines) to the accelerations determined by differentiating the velocity components measured by the GPS receiver and then transforming these to the *a*-frame (dashed red lines), from a portion of DEEPWAVE flight 15 that included a pitch maneuver, a speed run and a yaw maneuver at the times corresponding to the plot annotations.

turn direction	mean, $\langle \dot{\psi} \rangle$	std. dev. in $\langle \dot{\psi} \rangle$	mean, $\langle \dot{\psi}^* \rangle$	std. dev. in $\langle \dot{\psi}^* \rangle$
left	-1.821	0.001	-1.816	0.006
right	1.826	0.001	1.828	0.006

*Table 3: Comparison of the rate of change in heading ( $\dot{\psi}$ ) to the rate of change in the direction of the acceleration vector determined from differentiation of GPS-based velocity components ( $\dot{\psi}^*$ ). All units are [ ${}^\circ\text{s}^{-1}$ ]. The listed standard deviations are those estimated for the mean measurement.*

IRU gyros. Table 3 shows the comparison of rotation rates obtained in these two independent ways. The consistency between turn rates is remarkable, and a calibration representing both turn directions is  $\dot{\psi}_{cal} = a_0 + a_1 \dot{\psi}$  where  $a_0 = 0.003 \text{ s}^{-1}$  and  $a_1 = 0.999$ . Because the cosine of the mean roll angle was steady at 0.894, the corresponding calibration of BYAWR would use the first coefficient multiplied by 0.894; i.e.,  $\text{BYAWR}_{cal} = a_0^* + a_1 \text{BYAWR}$  where  $a_0^* = 0.003 \text{ s}^{-1}$ . This confirms that the offset in the measured rotation rate about the heading axis is small and the slope coefficient is indistinguishable from unity in this test.

Similar tests of the pitch and roll angles based on the GPS measurements are not possible. However, the critical test of the angle derivatives is to transform the measured derivatives for pitch, roll, and heading to the  $a$ -frame, with appropriate correction for inertial effects, and verify that the results match the measured rotation rates. The retrieval algorithm is discussed in a following section (Sect. 3.2.1) because it is also useful for obtaining surrogates for the body rotation rates in cases where they were not recorded or were not in the archive files. Plots and fits confirm that the transformed rotation rates obtained in this way match the measured rotation rates to within very small tolerances. For example, for the yaw rotation rate, a linear fit gives coefficients (-0.0003, 1.000001) for a fit of the transformed values to the measured values, with standard deviation smaller than  $0.01 {}^\circ \text{s}^{-1}$  and correlation coefficient 0.99997. Similar agreement was obtained for the pitch and roll angles. This is evidence that, as formulated in the code of the present document, the coordinate transformations and inertial corrections match those applied by the INS during the original mechanization.

As argued in Sect. 2.1, integration using the calculated derivatives and comparison to the INS-provided variables is the crucial test of the derivatives that the derivative function must pass if it is to be used in the Kalman filter. That is the topic of the next subsection.

## 2.4 Mechanization using the derivatives

The flight segment to be used to test the derivative function, from DEEPWAVE flight 15 3:20:00 to 3:55:00 UTC, included a “speed run” during which the aircraft airspeed varied from near-minimum to near-maximum (centered on 3:25:00 UTC), a maneuver with variation in sideslip angle, and four complete circles, two flown counterclockwise and two flown clockwise. To produce the right values of the state vector through these maneuvers is therefore a good test of the mechanization. Figure 2 shows that there is very good agreement for heading and roll, and pitch tracks well through a pitch maneuver (not shown) and the speed run, but there are

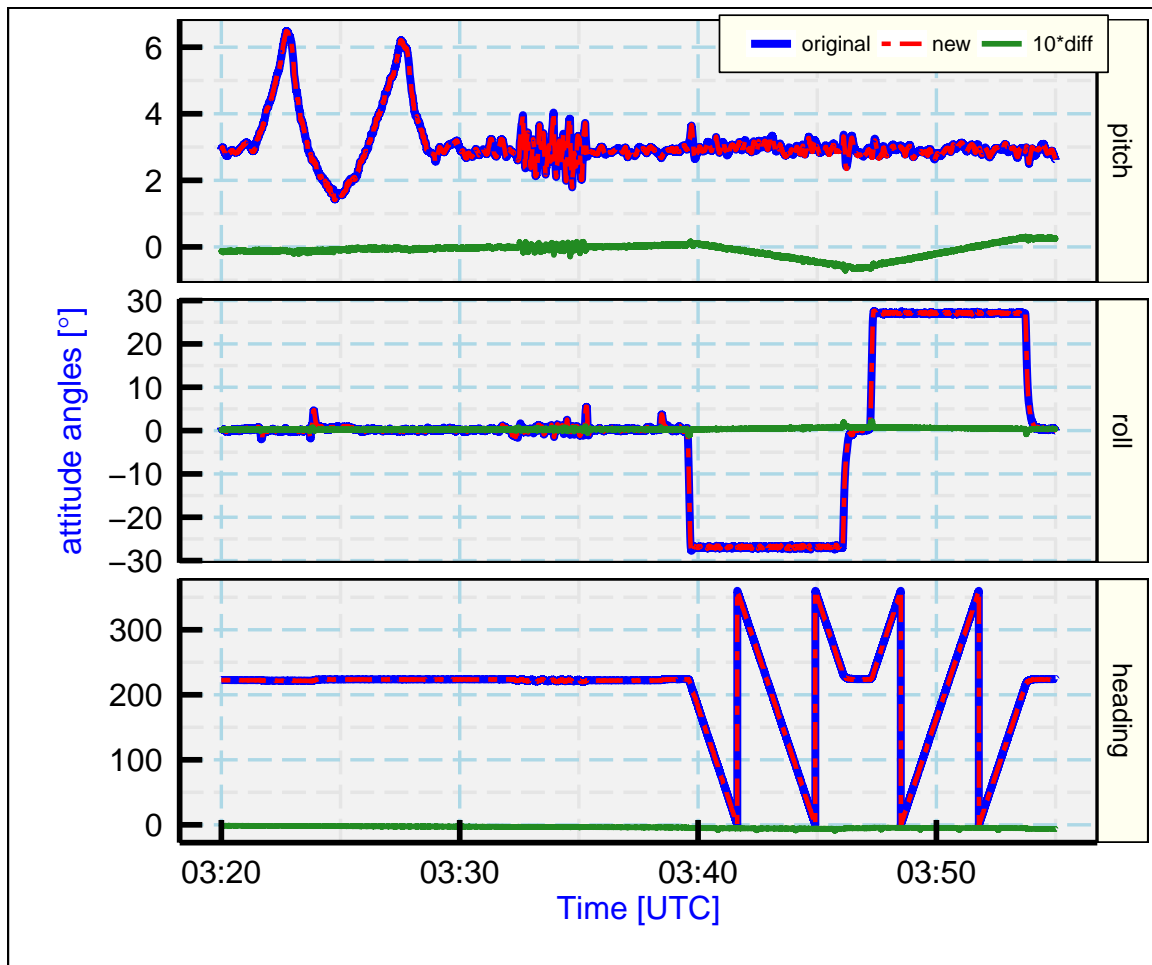


Figure 2: Comparison of INS-provided and integration-derived attitude angles, labeled "original" and "new", the latter plotted as dashed lines. The differences, multiplied by 10, are plotted as green lines.

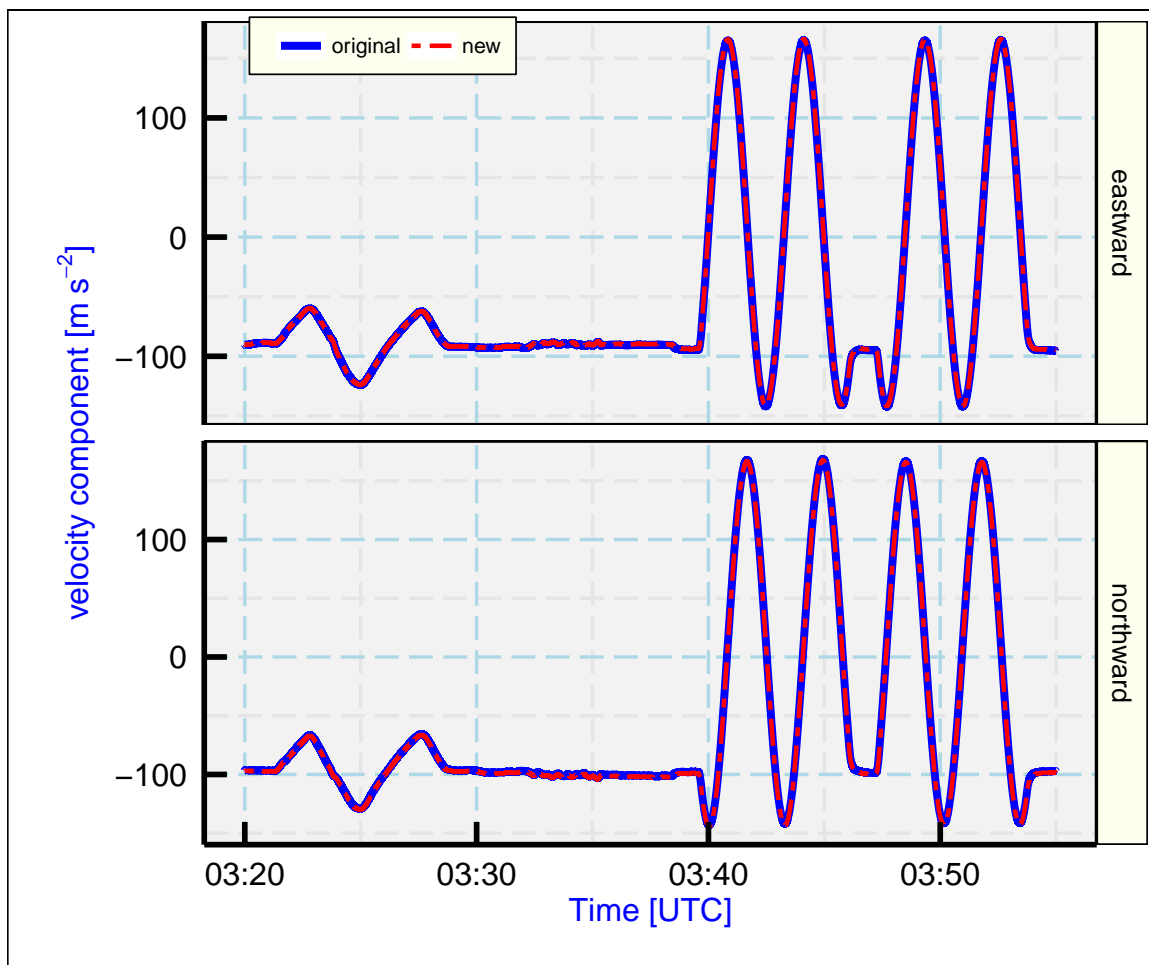


Figure 3: Comparison of INS-provided and integration-derived components of the aircraft velocity, the latter plotted as dashed red lines. The former are VEW, VNS and the latter VEWX, VNSX, for respectively the northbound and eastbound components of the aircraft velocity.

some small deviations between INS-provided values and the new values for pitch during the prolonged turns. The cause of this difference is not known, but it may be the result of residual timing differences or an internal calibration used by the INS or some difference in the inertial-correction terms, which become important in the turns. However, even after 5 min of turning, the accumulated difference is smaller than  $0.1^\circ$ , so this is not a serious weakness, especially because wind measurements from the GV are usually considered to have increased uncertainty in turns. Figure 3 shows that the ground-speed components tracked the INS values very closely through all the maneuvers. The key result is thus that as implemented above the derivatives of components of the state vector are approximately correct and integrate to values very close to those originally produced by the INS. The function providing those derivatives is therefore a reasonable basis for the Kalman filter that follows in Sect. 4.

## 3 Ancillary topics

### 3.1 A new variable for rate of climb

The integration provided by the INS includes variables for rate of climb (VSPD) and altitude (ALT), but both are updated using an algorithm that adjusts the altitude to the pressure altitude. This is not the variable needed for calculation of the vertical wind, and in baroclinic regions it is easy to detect the false variations that arise in rate of climb because of this updating scheme. The GPS-based variable GGVSPD can be used instead, but it is likely that the INS can produce a better representation of the high-frequency component, so it is useful to consider another variable based on the INS-provided measurements that can then be updated to GGVSPD via the Kalman filter.

The hydrostatic equation provides a basis for updating that is independent of the GPS:

$$\frac{dz}{dp} = -\frac{R_a T}{pg} \quad (4)$$

where  $z$  is the geometric altitude,  $p$  the pressure,  $R_a$  the gas constant for air,  $T$  the absolute temperature, and  $g$  the acceleration of gravity. Then

$$w_p = \frac{dz}{dt} = -\frac{R_a T}{pg} \frac{dp}{dt} \quad (5)$$

is the rate of climb in terms of geometric altitude. The random component of uncertainty in the pressure measurements makes this estimate too noisy to use directly, but it can be used to update the integrated vertical acceleration from the INS. Define these variables:  $w'_p$  as provided by (5) and  $w_p^* = \int_0^t a(t)dt$  where  $a$  is the vertical acceleration (ACINS) as provided by the INS. Define  $\Delta w_p = w'_p - w_p^*$  and the same variable after low-pass filtering to be  $\overline{\Delta w_p}$ . Then estimate the rate of climb of the aircraft from  $w_p = w_p^* + \overline{\Delta w_p}$ . The resulting rate of climb can then be integrated again, starting from a reference value provided by the GPS, to obtain a measure of altitude that, except for the initial reference, is independent of the GPS and is a useful representation of geometric altitude.

Implementation uses a Butterworth filter to find  $\overline{\Delta w_p}$ , as follows:

```
DIF <- WPPRIME - WPSTAR ## WPPRIME from hydrostatic equation,
## WPSTAR from integrating ACINS
DIF <- zoo::na.approx (as.vector(DIF), maxgap=1000, na.rm = FALSE)
DIFW <- signal::filtfilt (signal::butter(3, 2/tau), DIF)
ROC <- WPSTAR + DIFW
```

where the second statement removes missing values by interpolation and is needed to avoid an error exception in the third statement. The period of the filter cut-off is  $\tau$ , here selected after some exploration to be 300 s. The “`filtfilt()`” function filters by averaging two passes, forward and backward in time, to minimize phase-shift distortion of the filtered signal.

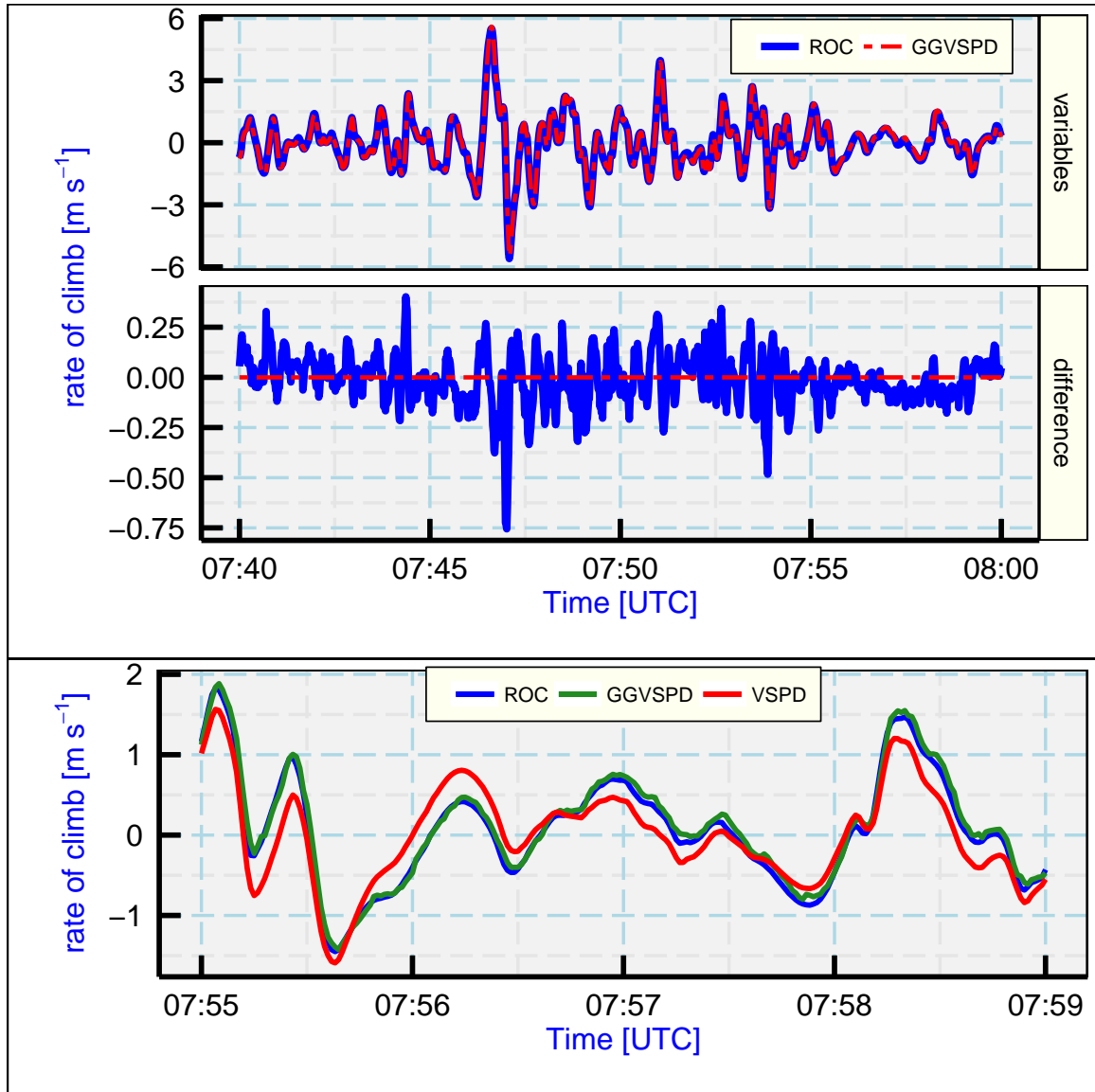


Figure 4: Comparison of a new variable representing rate of climb (ROC) to the GPS-based measurement (GGVSPD) and, in the bottom panel, the measurement provided by the INS (VSPD). The time covered in the bottom panel is a small segment from the time interval used for the top two panels.

The resulting variable “ROC” is plotted in Fig. 4 for comparison to the GPS-based variable GGVSPD. The bottom panel also shows the variable “VSPD” that is provided directly by the INS. The latter departs significantly from the other two variables, so using ROC as input to the Kalman filter appears preferable to using VSPD. The mean difference ROC–GGVSPD is 0.05, with standard deviation 0.12. ROC appears to vary more smoothly than GGVSPD, so Kalman-filter updating of ROC to GGVSPD may provide a better representation of aircraft rate-of-climb than GGVSPD. This will be considered further in Sect. 5, where the measurements of wind produced by the Kalman filter are discussed.

## 3.2 Retrieving IRU measurements by differentiation

### 3.2.1 Rotation rates

It is usually the case that the IRU variables for body rotation rate and body acceleration are not part of the data archives. Indeed, for all except recent projects and for all C-130 projects, these variables from the IRU were not even recorded in the original data tapes. Therefore, it is useful to be able to retrieve the accelerations and rotation rates from the measured variables present in those archive files. Differentiating the measured angles and velocity and then transforming the derivatives to the  $a$ -frame, with correction for the inertial effects as was discussed for the derivative of the state vector in Sect. 2.2, can provide retrieved values for the measurements. Then the Kalman filter can proceed using these surrogates for the original measurements.

For the rotation rates, the calculation proceeds as follows: (For additional detail, see the code in the R program chunk named `find-rotation-correction`. )

1. Start with an analytical expression for the derivative of the transformation matrix  $R_a^l$  in terms of attitude angles ( $\theta, \phi, \psi$ , pitch, roll, and heading) and their time derivatives  $\dot{\theta}, \dot{\phi}$ , and  $\dot{\psi}$ .
2. Use differences between sequential measurements of the attitude angles to find values for these time derivatives. Use these with the analytical expressions for the derivatives from step 1 to find the derivative of the transformation matrix from the  $a$ -frame to the  $l$ -frame.
3. Calculate the (minor) correction for inertial effects and *add* it to the derivative matrix of the transformation from the  $l$ -frame to the  $a$ -frame. (Normally this is subtracted during the forward transformation.)
4. Multiply the result by the  $l$ -frame-to- $a$ -frame transformation matrix. The result is a skew-symmetric representation of the measured rotation rates,  $\Omega_{ia}^a$ , from which the surrogate for the measurements can be extracted.

A mathematical expression of this algorithm, with  $\Omega_{il}^a$  representing the corrections for inertial effects,  $R_l^a$  the inverse of  $R_a^l$ ,  $\Omega_{ie}^l$  the effect of the rotation of the Earth, and  $\Omega_{el}^l$  the effect of translation of the  $l$ -frame, is as follows:

$$\dot{R}_a^l = R_a^l \Omega_{la}^a = R_a^l (\Omega_{ia}^a - \Omega_{il}^a) \quad (6)$$

$$\Omega_{ia}^a = R_l^a \dot{R}_a^l + \Omega_{il}^a \quad (7)$$

$$\Omega_{ia}^a = R_l^a \dot{R}_a^l + R_l^a (\Omega_{ie}^l + \Omega_{el}^l) R_a^l \quad (8)$$

(Noureldin et al. [2013]) where the left side of the last equation is the desired skew-symmetric representation of the rotation rate and all components of the right side are known, the time derivative from the differentiated measurements and the last term because it is the same correction for inertial effects used to find the attitude-angle derivatives from the measurements.

Figure 5 shows the resulting transformed derivatives, as the green lines, and the measured rotation rates as blue lines. They are mostly indistinguishable in these plots, and statistically they are nearly identical as characterized at the end of Sect. 2.3.2, so the transformed derivatives are valid estimates of the original rotation rates and should be suitable for use in the Kalman filter discussed in the next section.

### 3.2.2 Accelerations

The retrieval of accelerations is similar: Differentiate the  $l$ -frame velocity components {VEW, VNS, VSPD} to find the  $l$ -frame accelerations, apply the correction for inertial effects with sign opposite to that used for the  $a$ -frame-to- $l$ -frame transformation, then transform the results from the  $l$ -frame to the  $a$ -frame using the inverse of the transformation matrix used for the opposite transformation. See the workflow document for more detail, and refer to the code in the R chunk “checking-accelerations” for the R implementation. This is the same algorithm that was used in Sect. 2.3.1 to test the calibration of the accelerometers.

## 3.3 Simpler algorithms

### 3.3.1 Reasons for considering alternate algorithms

The Kalman filter discussed in the next section will produce estimated errors for the attitude angles, but it is possible to calculate a simpler estimate with some assumptions about the source of the error. One estimate was developed in Cooper et al. [2016], Sect. 6.4; cf. Eqs. 57. The intent of this section is to provide alternative corrections for all three attitude angles on the basis of relatively simple comparisons between measurements available from the combination of an INS and a GPS receiver. These corrections can be applied to archived data and so can lead to improvements in data collected in past as well as future projects, and they provide valuable comparisons to the results that will be obtained from the Kalman filter.

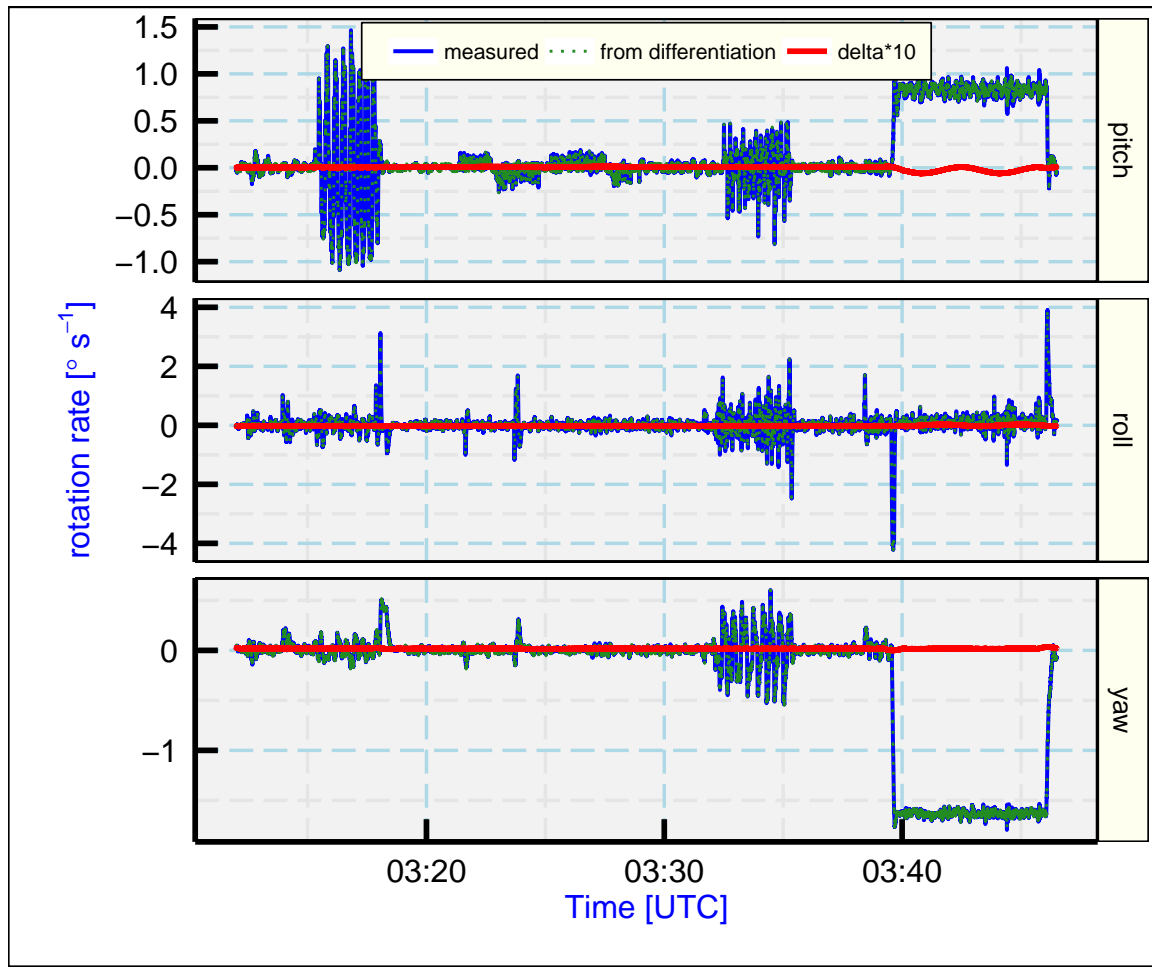


*Figure 5: Comparison of measured body rotation rates and those determined by differentiating the attitude angles. The red lines denoted as "delta\*10" show the difference between the two rates after multiplication by 10 to make the small differences visible. The measurements are from DEEPWAVE flight 15, from a portion of the flight that included, chronologically in the plot, maneuvers with rapid pitch variations, a speed run with slow pitch variations, a maneuver with rapid changes in sideslip, and two full left-turn circles.*

In the case of pitch and roll, the estimate of error relies on the derivatives of the errors in ground-speed components and position, which arise primarily from errors in those angles. For heading, the accelerations determined by differentiating the ground-speed components produced by the INS are compared to those determined by differentiating the GPS-based ground-speed components. This difference is dependent on the error in heading because the accelerations are measured in the  $a$ -frame and transformation to an Earth-reference frame (the  $l$ -frame) involves the heading. An error in heading results in a difference between the two sets of measured accelerations, and that difference can be used to detect the error in heading. As developed here, all corrections are applied to measurements after acquisition, not during recording or initial data processing, to be able to use algorithms that smooth measurements over centered intervals. This also makes it possible to correct archived data as long as the INS-provided and GPS-based measurements of ground speed are available.

### 3.3.2 Correcting the pitch and roll

An inertial system aligns during initialization to detect the local vertical direction and then calculates the new vertical direction as the aircraft moves (changing the local vertical direction) and accelerates (which can cause gyros to precess). Any misalignment present at initialization persists but also will oscillate and will cause errors in roll and pitch to mix as the aircraft changes flight direction. For the inertial system used on the NSF/NCAR GV, the standard uncertainty associated with this measurement is  $0.05^\circ$  in both roll and pitch (cf. [Cooper et al. \[2016\]](#)) for flight duration of a few hours, and the error often increases during the flight as heading errors and accelerometer biases affect the results.

The work of Schuler ([Schuler \[1923\]](#)) showed that coupling among some of these error sources leads to limits on the growth of errors and to simultaneous oscillations in some of the measurement errors. In particular, an error in pitch leads to an error in horizontal acceleration because gravity is resolved to have an erroneous horizontal component, and integration of that error in horizontal acceleration leads to a position error that grows so as to compensate for the false component of acceleration arising from the original error in pitch. However, when the error in pitch is reduced to zero, errors in position and velocity have been accumulated and those lead to growth of the error in pitch in the direction opposite to the original error. The result is a Schuler oscillation having a period of  $T_{Sch} = (R_e/g)^{0.5}/(2\pi) \approx 5064\text{ s}$  or  $84.4\text{ min}$ , where  $R_e$  is the radius of the Earth and  $g$  the acceleration of gravity.

The existence of this coupling allows estimation of the pitch error if the error in horizontal acceleration can be measured. That is the case if, in addition to the INS, there is a GPS receiver that can provide high-quality measurements of Earth-relative velocity. Modern GPS receivers, especially if they incorporate differential-GPS corrections or ionospheric corrections, produce velocity measurements that have remarkably low uncertainty, often a few cm/s, so these can be considered a standard against which to compare the corresponding INS-provided velocity. The difference between ground-speed components from the two systems thus determines the error in the INS-provided velocity and, after differentiation, the error in horizontal acceleration.

If  $a_n = a_n^* + \delta a_n$  where  $a_n^*$  is the true northward acceleration of the aircraft and  $\delta a_n$  is the erroneous acceleration that results from pitch and position errors, then the error in acceleration

(if the accelerometer error itself is negligible) is given by

$$\delta a_n^{(l)} = -g \delta \theta^{(l)} . \quad (9)$$

where  $\delta \theta^{(l)}$  is the error in pitch. The superscripts  $(l)$  denote that these pitch and acceleration errors are those present in the  $l$ -frame. Then the error in measured northward acceleration provides a direct measure of the error in pitch:

$$\delta \theta^{(l)} = -\frac{1}{g} \frac{d(\delta v_n^{(l)})}{dt} . \quad (10)$$

Because  $\delta v_n$  is measurable by comparison to measurements from a GPS receiver, the error in pitch can be found from (10). The analogous equation for the  $l$ -frame error in roll,  $\delta \phi^{(l)}$ , is

$$\delta \phi^{(l)} = \frac{1}{g} \frac{d(\delta v_e^{(l)})}{dt} . \quad (11)$$

The differentiated errors in the components of the aircraft ground speed thus provide estimates of the corrections to be applied to the measurements of pitch and roll. Because this correction relies on the observable effects of the errors in velocity, it is not sensitive to the source of the error, whether it arises from misalignment before flight, bias errors in the IRU gyros, or other sources except for these exceptions: (i) an error in measured acceleration from the accelerometers that contributes to the velocity errors in a way not dependent on the pitch or roll errors; and (ii) a minor dependence on error in heading that arises when the pitch and roll errors in the Earth-relative  $l$ -frame are transformed to the reference frame of the aircraft. The latter is negligible for normal heading errors, but the former can cause increasing amplitude or drift of the velocity errors. Plots of the observed errors in ground-speed components, shown later in this document, suggest relatively small changes in the amplitude of the Schuler oscillation during most flights, as would be expected if the accelerometer errors make only small contributions to the velocity errors.

An additional transformation of angles is needed to obtain the pitch and roll errors in the  $a$ -frame, the normal reference frame for these angles.<sup>4</sup> This calculation has been incorporated into a function “CorrectPitch ()” that is part of the “Ranadu” package. Given a data.frame containing appropriate measurements from a flight (specifically, VNS, VEW, GGVNS, GGVEW, LAT or LATC, GGALT, THDG, PITCH, and ROLL, representing respectively the eastward and northward velocity components of the aircraft as measured by the INS and the GPS receiver, the latitude, the altitude from the GPS, and the heading, pitch, and roll angle), the function returns estimates of the errors in pitch and roll. The workflow document accompanying this technical note provides additional detail on the algorithm used, and the R code is available in the file “PitchCorrection.R” in the Ranadu package, available at this URL: <https://github.com/WilliamCooper/Ranadu.git>, subdirectory “R”.

---

<sup>4</sup>The  $a$ -frame differs from the  $b$ -frame or body frame often discussed in the inertial-navigation literature by having  $\hat{x}$  and  $\hat{y}$  axes interchanged and the  $\hat{z}$  axis reversed to be downward, as is conventional for aircraft.

### 3.3.3 Correcting the heading

An algorithm related to that used for correcting pitch is developed here for estimating the error in heading. The basis for the correction is that an error in heading results in an error in transformation of the  $a$ -frame measurements of acceleration to the  $l$ -frame. These errors can be detected by comparing the actual acceleration of the aircraft (determined from derivatives of the GPS-based ground-speed components, as in the preceding section) to the measurements of acceleration after transformation to the  $l$ -frame.<sup>5</sup> If those measurements are not available, they can be retrieved by differentiating the corresponding ground-speed components provided by the INS, as discussed in Sect. 3.2.2.

The required transformation, developed by [Lenschow and Spyres-Duran \[1989\]](#) and others, involves a rotation about the roll axis to level the wings, a rotation about the pitch axis to level the longitudinal axis of the aircraft, and a rotation about the vertical axis as required to point the aircraft to the north. However, if there is an error in the heading ( $\delta\psi$ ) the last rotation will give final components  $a_{x,y,z}^{(l)}$  that have respective errors of  $\delta a_x^{(l)} = a_x^{(l)}(1 - \cos \delta\psi) - a_y^{(l)} \sin \delta\psi$ ,  $\delta a_y^{(l)} = a_y^{(l)}(1 - \cos \delta\psi) + a_x^{(l)} \sin \delta\psi$ , and  $\delta a_z^{(l)} = 0$  or, for small angles,

$$\begin{bmatrix} \delta a_x^{(l)} \\ \delta a_y^{(l)} \\ \delta a_z^{(l)} \end{bmatrix} = \begin{bmatrix} 0 & -\delta\psi & 0 \\ \delta\psi & 0 & 0 \\ 0 & 0 & 0 \end{bmatrix} \begin{bmatrix} a_x^{(l)} \\ a_y^{(l)} \\ a_z^{(l)} \end{bmatrix} \quad (12)$$

$$\delta a_x^{(l)} = -a_y^{(l)} \delta\psi \quad (13)$$

$$\delta a_y^{(l)} = a_x^{(l)} \delta\psi \quad (14)$$

$$\delta\psi = \frac{a_x^{(l)} \delta a_y^{(l)} - a_y^{(l)} \delta a_x^{(l)}}{(a_x^{(l)})^2 + (a_y^{(l)})^2} \quad (15)$$

The last equation is obtained<sup>6</sup> by minimizing the errors between the values of  $\delta a_i^{(l)}$  given by (13) and (14) and the measured error given by  $(a_i^* - a_i^{(l)})$ . This then gives an estimate of the rotation  $-\delta\psi$  that gives the best match between the measured accelerations and those determined from the derivatives of the GPS-based ground-speed components. The resulting value of  $\delta\psi$  from (15) is then an estimate of the error in heading. As in the pitch-correction algorithm, the acceleration vector  $\mathbf{a}^*$  is determined by differentiating the GPS-measured velocity components using Savitzky-Golay polynomials, , but with a 31 s span to avoid excessive distortion in 3-min turns. It was previously estimated that the uncertainty in a measurement of acceleration from differentiation of GPS-based measurements of velocity is not more than about  $0.01 \text{ m s}^{-1}/\tau$  where  $\tau$  is the time over which the average is calculated. For polynomials spanning 31 1\_Hz samples, the effective averaging time is about 20 s, leading to a minimum

<sup>5</sup>Additional small corrections arise from rotation of the Earth and rotation of the  $l$ -frame in an inertial frame, as discussed later..

<sup>6</sup>If the error measure to be minimized is  $\chi^2 = (\delta a_x + a_y \delta\psi)^2 + (\delta a_y - a_x \delta\psi)^2$ , differentiating  $\chi^2$  with respect to  $\delta\psi$  and setting the result equal to zero gives (15).

uncertainty of about  $0.0005 \text{ m s}^{-2}$ . Equation (15) indicates that, for an uncertainty in the heading correction of  $0.1^\circ$  or about 0.002 radians, the total horizontal acceleration should then be at least  $0.0005/0.002=0.25 \text{ m s}^{-2}$ .

Typical horizontal accelerations in turns exceed  $4 \text{ m s}^{-2}$  in the  $l$ -frame, but horizontal accelerations exceeding  $1 \text{ m s}^{-2}$  are seldom encountered outside of turns. Therefore, the algorithm developed here only provides a valid correction if there are regular turns during the flight. In the following, heading corrections will be calculated only when the horizontal acceleration exceeds  $1 \text{ m s}^{-2}$  to avoid excessive noise and uncertainty. For a flight that transits in a straight line from start to finish, attempts to use these estimates are cannot be useful. Fortunately, in most research flights there are many turns, e.g., as the aircraft flies back and forth over a mountain range or flies fixed raster patterns for mapping. Each turn can provide significant horizontal accelerations that give estimates of the heading error, but these estimates are only sporadic and must be linked by extrapolation to obtain valid corrections spanning intervals without significant acceleration. The heading correction therefore has a higher uncertainty than the pitch correction and, unlike the pitch correction, depends on particular flight maneuvers for successful operation. In addition, unlike the pitch error, the heading error is not coupled to other errors in ways that limit its growth, so determining an estimated correction is important not only to provide improved measurements but also to determine the estimated magnitude of the uncorrected error.

The requirements for valid results from this algorithm are as follows:

- The flight path must include maneuvers that provide horizontal accelerations, usually turns of at least 30 s duration *in each direction*. The reason is that it is difficult to correct for timing errors in the measurements of heading relative to the measured ground-speed components from a GPS receiver, and even a delay of 50 ms will, for a turn rate corresponding to a three-minute turn through  $360^\circ$ , lead to a  $0.05^\circ$  false indication of a heading error. However, the error reverses sign with the direction of the turn, so averaging the results from left turns and from right turns will correct for this false indication of a heading error. Course-reversal maneuvers like “90-270” turns ( $90^\circ$  one direction followed by  $270^\circ$  the other direction) provide good data for this algorithm, as do “60-300-60” teardrop turns that are a faster means of returning to the starting point. If wind measurements are critical to the research, it may be useful to include patterns like “S” turns periodically, with 30 s turns in opposite directions, to provide the needed accelerations.
- To the extent possible, sampled time series should be corrected for sampling delays. The most important such correction is the timing of the heading measurement from the INS relative to the ground-speed measurements from the GPS receiver. In the examples shown in this note, the differences between different turn directions were minimized by shifting the heading forward in time by 92 ms. The averaging provided by the first item above helps reduce errors from timing, but it is still preferable to keep those errors small. Full-circle patterns flown in each turn direction provide a sensitive test of timing errors.

Many research flights and research data sets meet these requirements, and where wind measurement is important appropriate flight maneuvers can be incorporated into flight plans for future

projects. The algorithm implemented here, for which R code is available in the “Ranadu” package (cf. <https://github.com/WilliamCooper/Ranadu.git>, directory “R”, script “HeadingCorrection.R”), includes these components:

1. *Shift the timing of the heading measurement as needed to match the GPS-receiver measurements of ground velocity.*
2. *Differentiate the ground-speed measurements provided by a GPS receiver, using third-order Savitzky-Golay polynomials spanning 21 s, to obtain reference measurements of horizontal accelerations in the  $l$ -frame.*
3. *Transform the accelerations measured by the INS in the  $a$ -frame to the  $l$ -frame. Filter these results also using Savitzky-Golay polynomials of the same order and span so that they are smoothed in the same way as the ground-speed derivatives.*
4. *Use (15) to obtain estimates of the heading error  $\delta\psi$  at each time.* However, apply data restrictions to avoid cases of high uncertainty. The most important restriction used here was to require that the total horizontal acceleration in the  $l$ -frame be larger than  $1 \text{ m s}^{-2}$ .
5. *Use a search algorithm to identify flight segments with turns* (specifically, magnitude of roll larger than  $10^\circ$ ) continuously except for possible gaps of 5 min. Require that these flight segments have both right and left turns, with at least 25 s of each.
6. *For each such segment, calculate the mean correction and its standard deviation and the mean time for each turn direction.*
7. *Use cubic spline interpolation to represent the heading correction over the course of the flight.*
8. *Subtract the result given by this interpolation from the measured heading to obtain the corrected heading.*

### 3.3.4 Results from the simple correction algorithms

Results will be presented later in comparison to the results from the Kalman filter. See Figs. 9 and 11.

## 3.4 Angle of attack

As described in Cooper et al. [2016], the standard empirical representation of angle of attack has been

$$\alpha = c_0 + \frac{\Delta p_\alpha}{q} (c_1 + c_2 M) \quad (16)$$

where  $\Delta p_\alpha$  is the pressure difference measured on the radome between top and bottom ports,  $q$  is the dynamic pressure and  $M$  is the Mach number calculated from the measurements of

dynamic and static pressure before static-defect corrections are applied. The coefficients were found by fitting that formula to a reference value  $\alpha^*$  that assumes there is zero vertical wind:

$$\alpha^* = \theta - \frac{w_p}{V} \quad (17)$$

where  $\theta$  is the pitch angle,  $w_p$  the rate of climb of the aircraft and  $V$  the airspeed.

An alternate approach is developed here. The reference value as given by (17) is split into two components,  $\alpha^* = \alpha_f^* + \alpha_s^*$  that result from applying a Butterworth low-pass filter to  $\alpha^*$  (in the code, the variable AOAREF) to obtain  $\alpha_s^*$  and then finding  $\alpha_f^*$  from  $\alpha_f^* = \alpha^* - \alpha_s^*$ , where the  $f$  and  $s$  subscripts represent the high-pass and low-pass components after filtering. These components are then represented by separate fits:

$$\alpha_f = c_1 \left( \frac{\Delta p_\alpha}{q} \right)_f = c_1 \left( \frac{\{\text{ADIFR}\}}{\{\text{QCF}\}} \right)_f \quad (18)$$

$$\alpha_s = d_0 + d_1 \left( \frac{\Delta p_\alpha}{q} \right)_s + d_2 q_s = d_0 + d_1 \left( \frac{\{\text{ADIFR}\}}{\{\text{QCF}\}} \right)_s + d_2 \{\text{QCF}\}_s \quad (19)$$

where the second equalities in each line reference the standard variable names used in netCDF archives to represent the corresponding quantities in the first equality. More complicated representations were tested in both cases, but these appear to provide adequate fits without additional terms.

This approach has a substantial advantage over the approach in standard use. The important sensitivity to fluctuations is not compromised by efforts to represent the slowly varying zero level for angle of attack, and the slowly varying offset can be represented by more complex equations without having those added factors influence the high-frequency response. The result is an empirical representation that is appropriate for all recent GV projects and that does not need to be changed for each project, as has been the case for many recent projects that use the standard representation.

To find the coefficients in (18) and (19), a composite data set was constructed from most flights from three recent projects, ORCAS, CSET, and DEEPWAVE.<sup>7</sup> A full description of how these coefficients were determined is contained in [this document](#), and the coefficients from that analysis are used here. They are  $c_1 = 21.481$  and  $\{d\} = \{4.5253, 19.9332, -0.00196\}$ . Then the variables entering the fits in (18) and (19) were obtained by using a low-pass Butterworth forward-and-backward filter to find the slowly varying components  $(\Delta p_\alpha/q)_s$  and  $q_s$ , and the first was subtracted from the unfiltered variable to find  $(\Delta p_\alpha/q)_f$ . The new angle-of-attack variable was then calculated from  $\alpha = \alpha_f + \alpha_s$ .

This calculation gave much less variation from project to project and within projects and seemed to provide a standard representation applicable to all recent GV projects since a change was made to the radome.

---

<sup>7</sup>For descriptions of these projects, see the EOL web site at [this URL](#).

## 4 The Kalman filter

### 4.1 The algorithm used

Section 2.4 verified that a valid representation of the derivatives of the state vector is available. An error-state Kalman filter that uses that derivative function is described in this section. The computational algorithm has these components:

1. The first step is to initialize an error-state vector  $\delta\mathbf{x}$  from initial measurements of the differences between the INS and GPS-based values of position and velocity. Other errors in components of the state vector are unknown at the start of the integration and so will be initialized as zero. The 15-component vector used here contains the respective errors in latitude, longitude, altitude, eastward ground speed, northward ground speed, rate of climb, pitch, roll, heading, pitch-axis rotation rate, roll-axis rotation rate, yaw-axis rotation rate, lateral component of acceleration, longitudinal component of acceleration, and normal component of acceleration. The rotation-rate errors and acceleration errors in this error-state vector are biases; random errors enter instead through the noise-covariance matrix  $\mathbf{Q}$  below.
2. The covariance matrix  $\mathbf{V}$  characterizing the errors in the error-state vector is also needed. This is here initialized to have rather large components corresponding to the INS-provided measurements because it is expected that the GPS measurements will have much lower uncertainty than these INS-provided components and that will constrain the covariance matrix during the calculation.  $\mathbf{V}$  is initialized as a  $15 \times 15$  diagonal matrix where the diagonal elements are the squares of these values:  $\{2000/R_m, 2000/(R_n \cos \lambda), 500, 2, 2, 2, 0.3^\circ, 0.3^\circ, 1^\circ, 0.005^\circ s^{-1}, 0.005^\circ s^{-1}, 0.005^\circ s^{-1}, 0.0005, 0.0005, 0.0005\}$ . All entries are in SI units except those where units are listed as degrees, and those cases are converted to radians before use. The variables  $R_m$  and  $R_n$  are appropriate radii of the Earth, as discussed in Sect. 2.2, and  $\lambda$  is the latitude. The initial values assigned to this covariance matrix have little effect on the results because the covariance matrix is updated during the calculation based on the other error estimates.
3. The function “STMFV” was verified above and so provides appropriate derivatives of the state vector, for the first nine components. The error-state vector, however, also includes errors in the additional six components representing the rotation-rate and acceleration vectors. The derivatives of the first nine components depend on the derivatives of the additional six components, so all 15 elements in the error-state vector must be considered. For an error-state Kalman filter, the forward propagation of the error state can be found from the Jacobian  $\mathbf{J}(\mathbf{x})$  of that derivative function of the state vector, so the error-state transition matrix  $\mathbf{T}$  is the sum of that Jacobian (multiplied by the time step) and the 15-element diagonal matrix:

$$\delta\mathbf{x}_k = \mathbf{T} \delta\mathbf{x}_{k-1} = (\mathbf{J}(\mathbf{x}_{k-1}) \Delta t + \mathbf{I}) \delta\mathbf{x}_{k-1} \quad (20)$$

The derivative function must be extended for this use beyond that used for mechanization, because the dependence of the first nine components on the additional six components is

needed for the complete Jacobian. Furthermore, the dependence of the additional six derivatives on each other and the first nine components is needed. This is added as follows:

- (a) Expanding the state-vector  $\mathbf{x}$  to include all 15 components naturally includes the effect of the added six components on the first nine components because the derivative calculation outlined earlier already includes these dependencies. The corresponding components of the Jacobian will therefore be included naturally.
  - (b) The dependence that is not included in that case is the dependence of the derivatives of the last six components on the values of the first nine. There is no such dependence, though, because these are direct measurements in an inertial frame and so are not affected by other components of the state vector. The changes in the errors in acceleration or rotation rate do not depend analytically on any other part of the error-state vector, so the terms in the Jacobian involving these components will be zero. This arises naturally if the state vector is expanded to 15 components and then used to calculate the Jacobian numerically. There will be new terms in the Jacobian describing how, for example, a derivative of a velocity component changes with the change in a component of acceleration, but not the reverse component describing how the derivative of a component of acceleration changes with the change in velocity component. The highest  $6 \times 6$  submatrix in the Jacobian will have 0 for all terms.
  - (c) Implementation then involves having the derivative function return a 15-component derivative where the first nine components are as before and the last six components are zero. Using that derivative function to find the Jacobian will then include terms that involve all the components and so describe the full interdependence of the errors. For example, errors in the rotation-rate components will affect all of the error terms for the first nine components and so will enter most of the Jacobian terms involving the derivatives of the first nine components with respect to the rotation-rate components.
4. The noise-covariance matrix  $\mathbf{Q}$  represents the estimated noise in the INS forward integration. The results vary significantly with different choices for these values, and the choices made here are the result of tuning to find a set of values giving reasonable results. The 15 values used for the diagonal components of this matrix are the squares of the following:  $\{a/R_m, a/(R_n \cos \lambda), a, 0.02 \text{ m s}^{-1}, 0.02 \text{ m s}^{-1}, 0.05 \text{ m s}^{-1}, 0.01^\circ, 0.01^\circ, 0.01^\circ, 0.02^\circ/\text{s}, 0.02^\circ/\text{s}, 0.02^\circ/\text{s}, 0.00005 \text{ m s}^{-2}, 0.00005 \text{ m s}^{-2}, 0.00005 \text{ m s}^{-2}\}$  where  $a$  is 10 m. Cases with units of degrees are converted to radians before use. These values are used with a 5-s time step, and they may need adjustment if a different time step is used. To estimate these values, a high-pass filter of high-rate measurements for a straight-and-level flight segment was used to find the standard deviation of such signals applicable at a 0.2 Hz sample rate, corresponding to the 5-s time step used in this particular implementation of the Kalman filter. For positions, this approach indicated that appropriate values would be about 10% of the listed values, but the listed values were used instead because the smaller values tended to result in numerical singularities in the inversion required in step 6 below. This change did not otherwise result in any significant change in the solution. In the case

of accelerations, the variance spectra for these measurements show characteristics of a noise limit at an amplitude of about  $0.001 \text{ m s}^{-2}$ . However, this appears to arise from the resolution with which the variables were recorded, so the forward integration in the INS may use less noisy measurements. When a noise estimate this large was used in the following calculations, substantial errors in pitch and roll were predicted that seemed unrealistic and were reduced substantially if these noise estimates were reduced. The very low values listed above for these elements of the noise-covariance matrix correspond to assuming that the noise affecting the accelerometers is negligible, and indeed setting these values to zero gives almost the same result as that obtained by using these small values. The Kalman filter does estimate non-zero bias in accelerations during the integration, so very small noise estimates still permit compensation for errors in the accelerometers. All the values listed may be higher than the true noise, but at least they should be upper limits.

5. Once  $\mathbf{T}$  and  $\mathbf{Q}$  are specified, the covariance  $\mathbf{V}$  matrix can be updated each time step via<sup>8</sup>

$$\mathbf{V} = \mathbf{T} \mathbf{V} \mathbf{T}^T + \mathbf{Q} \quad (21)$$

6. The Kalman gain is then given by

$$\mathbf{K} = \mathbf{V} \mathbf{H}^T \left\{ \mathbf{H} \mathbf{V} \mathbf{H}^T + \mathbf{R} \right\}^{-1} \quad (22)$$

where  $\mathbf{H}$  is a  $15 \times 6$  diagonal matrix representing how the six measured differences (GPS-INS) correspond to the error-state vector.  $\mathbf{R}$  is the measurement-noise covariance matrix representing the noise in the GPS-based measurements, a  $6 \times 6$  matrix having diagonal elements that are the squares of these components:  $\{0.5/R_m, 0.5/(R_n \cos \lambda), 0.5, 0.02, 0.02, 0.05\}$  in SI units. These were based on the same analysis used to determine estimates for the components of  $\mathbf{Q}$  and represent very high confidence in the measurements from the GPS receiver. The particular time interval was one where [OmniSTAR corrections](#) were available, so this represents the best performance that can be expected from the GPS receiver. An additional seventh component, based on an estimate of the heading error determined from (15) above, will be discussed below and added to the matrices so that  $\mathbf{H}$  will be  $15 \times 7$  and  $\mathbf{R}$  will be  $7 \times 7$ .<sup>9</sup>

7. Define  $\delta \mathbf{z}$  as the set of six measurements consisting of the differences between GPS and INS-provided position and velocity. Because the GPS antenna on the GV is located  $L_G = 4.3 \text{ m}$  behind the INS, a small correction is made to the velocity differences to account for the rotation rate of the aircraft:

$$\begin{aligned} \delta z_4 &= v_e - v_e^{(G)} - L_g \dot{\psi} \cos \psi \\ \delta z_5 &= v_n - v_n^{(G)} + L_g \dot{\psi} \sin \psi \end{aligned} \quad (23)$$

---

<sup>8</sup>Matrix multiplication is indicated by adjacent matrices separated by spaces. The corresponding symbol in R is '%\*%' but transposition is sometimes required because matrices are represented in R in column-major format.

<sup>9</sup>Three additional measurements were explored for inclusion, the three measurements of acceleration determined by differentiating the measurements of velocity components from the GPS receiver. These complicate the tuning and did not appear useful, so they will not be discussed in this technical note. Their inclusion in the solution appears to be redundant.

$$\delta z_6 = v_u - v_u^{(G)} - L_G \dot{\theta} \cos \phi$$

where  $\{v_e, v_n, v_u\}$  are the eastward, northward, and upward components of the aircraft velocity as measured by the INS, the same symbols with superscript (G) are the corresponding measurements from the GPS receiver,  $\psi$  is the heading,  $\phi$  the roll angle, and  $\dot{\psi}$  and  $\dot{\theta}$  are the respective time derivatives of the heading and pitch angles. Similar corrections are made to the horizontal position differences. The error-state vector is then further updated as follows:

$$\delta \mathbf{x}_k \leftarrow \delta \mathbf{x}_k + \mathbf{K} \{ \delta \mathbf{z} - \mathbf{H} \delta \mathbf{x} \} \quad (24)$$

8. Finally, the covariance matrix is updated further according to

$$\mathbf{V} \leftarrow \mathbf{V} - \mathbf{K} \mathbf{H} \mathbf{V} \quad (25)$$

To apply these equations, it is not necessary to use a high-rate data file and update at high rate because it is expected that the errors vary slowly. However, turns and other maneuvers can introduce spurious effects if time delays are not adjusted well. For these reasons, a 1-Hz data file will be used for the following example, and the measurements of components of the velocity and of the attitude angles as well as the rotation rates and accelerations will be shifted in time where needed and then smoothed before applying the Kalman filter. DEEPWAVE flight 16 (4 July 2014) was selected, and the measurements were filtered with 11-s smoothing of accelerations and 301-s smoothing of measured velocity components and attitude angles. A 5 s update interval was used for the example that follows.

The file “KalmanFilterTechNote.Rnw” loads R “chunks” from a directory named “chunks” when it runs, so this directory is archived along with the file. The reason is that a separate R script designed to support interactive runs, with specification of the archive file to be used and with options to change time shifts and calibrations but which omits generation of the text and plots in this technical note, can use those same chunks. That script is called “KalmanFilter.R”, and the workflow document includes detailed instructions for its use.

## 4.2 Detecting the error in heading

Most of the components of the state vector have good feedback from GPS-based measurements, but an exception is the measurement of heading. For position and velocity, there is direct correspondence between INS-provided and GPS-based measurements. For pitch and roll, there is strong coupling to errors in the eastward and northward components of aircraft velocity. However, the coupling of INS-provided heading to GPS-based measurements is not a case of strong coupling (to which the Schuler oscillation applies), and it is less effective to update via measurements from the GPS receiver. To improve the constraint on heading, another approach was tried that estimates the error in heading by using derivatives of the measurements provided by the GPS receiver. The basis for this approach is related to that discussed in Sect. 3.3.3, in particular via (15) which estimates the error in heading by comparing the directions of the two accelerations that arise in the first case from transforming the IRU-measured accelerations to

the  $l$ -frame and in the second by differentiating the GPS-based components of the aircraft velocity. The latter direction then provides a reference toward which the former can be updated. Unfortunately, the measured accelerations are too noisy for this to be effective except during turns, so updating to this reference value must consider the variance in the estimated error.

Most of the evidence from flights that have been examined suggests that the heading error is small and changes little during the flight. (The evidence comes primarily from comparisons among independent inertial navigation systems, as discussed in [Cooper et al. \[2016\]](#).) However, the Kalman filter often leads to estimates of heading error that are  $0.2^\circ$  or more, accompanied by large variances that indicate substantial uncertainty in the estimates. The heading error is constrained well only during turns, when there are significant horizontal accelerations. With strong accelerations, the direction of the acceleration is determined well and can be used as an additional error term in the Kalman filter. Although inclusion of this term is redundant in theory because the filter already determines optimal corrections to minimize the measurement errors, specific inclusion of this term did lead to apparent improvement in performance, particularly the reduction of noise in the estimated heading error and smaller excursions from the mean correction.

Because significant horizontal accelerations occur mostly in turns when the heading angle is changing rapidly, it is very important to have correct relative timing between the INS-provided measurement of heading and the GPS-based measurement of velocity.<sup>[10](#)</sup> The GPS measurements are assigned correct times by the GPS receiver and so provide a standard clock against which to compare other measurements.<sup>[11](#)</sup> If the GPS-vs-INS time shift is not removed, a bias will be introduced into the heading correction that varies with turn direction. Therefore the following procedure was followed to remove this time shift:

1. Differentiate the GPS-based measurements to obtain  $\dot{v}_e$  and  $\dot{v}_n$ .
2. Transform the unshifted body accelerations to the  $l$ -frame, with rotation-rate corrections, to obtain the eastward and northward components of acceleration ( $a_e^{(l)}$ ,  $a_n^{(l)}$ ) in the local-level frame ( $l$ -frame).
3. Find the heading correction for unshifted measurements by calculating  $\delta\psi$  from [\(15\)](#).
4. Calculate the running-standard deviation of  $\delta\psi$  spanning 30 seconds. Select the subset of  $\delta\psi$  for which that standard deviation is less than  $0.2^\circ$ .
5. Fit the subset to find the slope  $b$  in the relationship  $\delta\psi = a + b \tan\phi$  where  $\phi$  is the roll angle. The rate of turn  $R$  is related to the roll angle  $\phi$  according to the relationship  $R = g \tan\phi/V$  where  $V$  is the airspeed, so  $\tan\phi = RV/g$  and  $\delta\psi = a + bRV/g$ . A time delay of  $\delta t$  produces a heading error of  $-R\delta t$ , so  $-R\delta t = a + bRV/g$  and the time shift can be estimated from

---

<sup>[10](#)</sup>As an illustration, a 50-ms delay in heading during a 3-min turn causes a shift in heading relative to the correct time of  $0.1^\circ$ , so adjustment to at least this uncertainty is desirable.

<sup>[11](#)</sup>It appears that the relative timing between the IRU and the GPS receiver can change enough during some flights to introduce additional errors that are sometimes detectable. This warrants further study.

$$\delta t = -b \frac{V}{g} . \quad (26)$$

For example, for DEEPWAVE flight 16,  $b = 0.2146^{\circ}\text{s}^{-1} = 0.003745 \text{ rad s}^{-1}$  and  $V \simeq 240 \text{ m s}^{-1}$ , so (with  $g=9.8 \text{ m s}^{-2}$ )  $\delta t = -0.092 \text{ s}$ . The negative sign indicates that the INS-provided measurement of heading appears to be shifted backward (earlier) in time by 92 ms relative to the GPS-based measurements of aircraft velocity. The standard error from the fit indicates that this shift was determined with an uncertainty of about 3 ms, so this is a very sensitive way to determine the time shift. Note that the result is not influenced by a real error in heading.

6. Apply this time shift to the measurements of ground speed from the GPS (GGVEW and GGVNS), in this case shifting them backward (earlier) in time by 92 ms while leaving the heading unshifted.<sup>12</sup> For a data file containing measurements at 1 Hz, this requires creating an interpolated high-rate vector of measurements, shifting that vector, and then extracting a shifted 1-Hz vector from the shifted measurements. The Ranadu function ShiftInTime() accomplishes this by interpolating to a 125-Hz variable.

After an appropriate time shift is introduced, (15) is an appropriate measurement of heading error to include in the error-measurement vector  $\delta z$ . Here, that is accomplished by adding a seventh component to the measurement vector and a seventh row to the observation matrix  $H$ , where a matrix element 1 then appears in row 7, column 9, to associate this measurement with the heading angle. In normal straight flight, the standard deviation in the estimate obtained from (15) is around  $15^{\circ}$ , but in turns this standard deviation reduces to typically about  $0.15^{\circ}$ . This has two important consequences. First, flights without turns or other sources of horizontal acceleration will lack the information for adjusting the heading, so in flights where good wind measurements are important regular turns should be part of the flight plans. Second, when the GPS-based estimate of the heading error is used, an appropriate variance should be assigned to prevent excessive noise from affecting the result from the Kalman filter. It appears best to suppress updating to the GPS result entirely for this seventh term except when horizontal accelerations are significant (more than  $1 \text{ m s}^{-2}$ , which is common only in turns where accelerations are often about  $3 \text{ m s}^{-2}$ ), and the case to be shown used this suppression of updating. Then the running variance in the estimate of heading error can be used as the appropriate factor to include in the noise matrix  $R$ . For the flight being used as an example, the mean and standard deviation of the correction from (15) for all cases where the horizontal accelerations exceed this criterion are  $0.003 \pm 0.15^{\circ}$  for 4295 1-Hz measurements, and the mean error is determined to a standard uncertainty of about  $0.002^{\circ}$ .

---

<sup>12</sup>The reason that it is preferable to shift GGVEW and GGVNS rather than THDG is that it is common in data archive for heading to already be shifted. In the case discussed here, heading was already shifted by  $-80 \text{ ms}$ . However, this was done after processing by the INS, so measurements like VEW and VNS have been determined with the heading as used internally by the INS, not as shifted during subsequent processing. The feedback provided by the Kalman filter then relies on the heading before shifting, and subsequent shifting of the heading has no effect on those measurements. It does affect the recalculated transformation from  $a$ -frame to  $l$ -frame, so there would be an inconsistency between (15) and other estimates of the heading error arising from the Kalman filter.

### 4.3 Smoothing the errors in pitch and roll

Because the errors in pitch and roll are strongly coupled to the errors in velocity, good estimates of these errors should arise naturally from the Kalman filter. However, the estimated errors so obtained are noisy in comparison to the direct measurements, so application of those corrections will introduce undesirable noise into the results from the filter. Variations in the errors in velocity indicate that the main source of error in pitch is expected to be the slowly varying Schuler oscillation, so it is preferable to smooth the corrections before applying them to the original measurements to avoid the introduction of noise. As described above, the errors in pitch and roll are those that apply to the original measurements in the  $a$ -frame. However, if a major source of those errors is platform misalignment that varies slowly, the errors will vary smoothly in the  $l$ -frame, where  $l$ -frame pitch error refers to platform north-south tilt and  $l$ -frame roll error refers to platform east-west tilt. In the  $a$ -frame, each turn leads to mixing of the pitch and roll errors and to abrupt changes, so smoothing in the  $l$ -frame followed by transformation back to the  $a$ -frame produces a better result. This will be discussed further after the results from the Kalman filter are presented.<sup>13</sup>

---

<sup>13</sup>An alternative that would likely be preferable would be to use the  $l$ -frame errors in pitch and roll in the state vector. This has not been done in this document and the associated code, but might be worth exploring in the future because it should produce smoother variations in the corrections.

## 4.4 Results

### 4.4.1 Position

Because the time step for the Kalman filter is normally longer than the interval between measurements in the original file, the error estimates from the Kalman filter are interpolated to the original data rate and then subtracted from the original measurements to obtain corrected results corresponding to the original measurements. The corrected results for position, after conversion to meters, are shown in Fig. 6 for DEEPWAVE flight 16. The blue lines in the top two panels show that differences between the corrected (KF) and GPS-based measurements ( $\text{DLAT} = \text{LAT} - \text{GGLAT} + \text{CLAT}$  and  $\text{DLON} = \text{LON} - \text{GGLON} + \text{CLON}$  where CLAT and CLON are the corrections produced by the Kalman filter) are negligibly small for latitude and longitude, at the resolution of these plots. This good agreement arises from the corrections CLAT and CLON shown as the green lines, which show a smoothly varying Schuler oscillation.<sup>14</sup> Using the new variable ZROC from Sect. 3.1 for altitude leads to only a small offset in vertical position; this would be 100 times larger if the INS-provided variable ALT had been used, because then the correction would need to remove the difference between pressure altitude, used by the INS, and geometric altitude from the GPS.

At higher resolution than plotted here, there are step-change features in the KF result that are not present in the GPS measurement, at a level of about 10 m. The reason is that this is the resolution at which the original measurements from the INS (variables LAT and LON) are recorded, so a smoothly varying correction as provided by the Kalman filter preserves these step changes. Because the true values of latitude and longitude are not expected to show high-frequency components at these frequencies, the positions after correction are further filtered using a low-pass Butterworth filter with a cutoff frequency corresponding to about 10 s. This effectively smooths the jumps arising from the original measurements from the INS and leads to agreement between the KF and GPS-based values corresponding to about 10 m standard deviation for the part of the flight track that excludes the initial climb and final descent. Some part of this standard deviation likely arises from minor time shifts between the measurements from the INS and GPS.

The result then is that the positions after correction are in agreement with the GPS-based measurements of position to within about 10 m in each component of the position vector. The uncertainty arising from the calculated covariance matrix also indicates uncertainty for individual measurements of latitude or longitude corresponding to about 10 m.

### 4.4.2 Ground-speed components and rate of climb

Figure 7 shows the corresponding differences between the aircraft-velocity components and the GPS-based measurements, for the same flight as that shown in the preceding figure. For the two horizontal components of ground speed, the mean difference between KF and GPS results

---

<sup>14</sup>Before addition to the original measurement, this correction has been filtered using a three-pole low-pass Butterworth filter with cutoff frequency corresponding to a period of 600 s. This avoids the introduction of noise from the Kalman filter that otherwise would contaminate the high-frequency variance spectra.

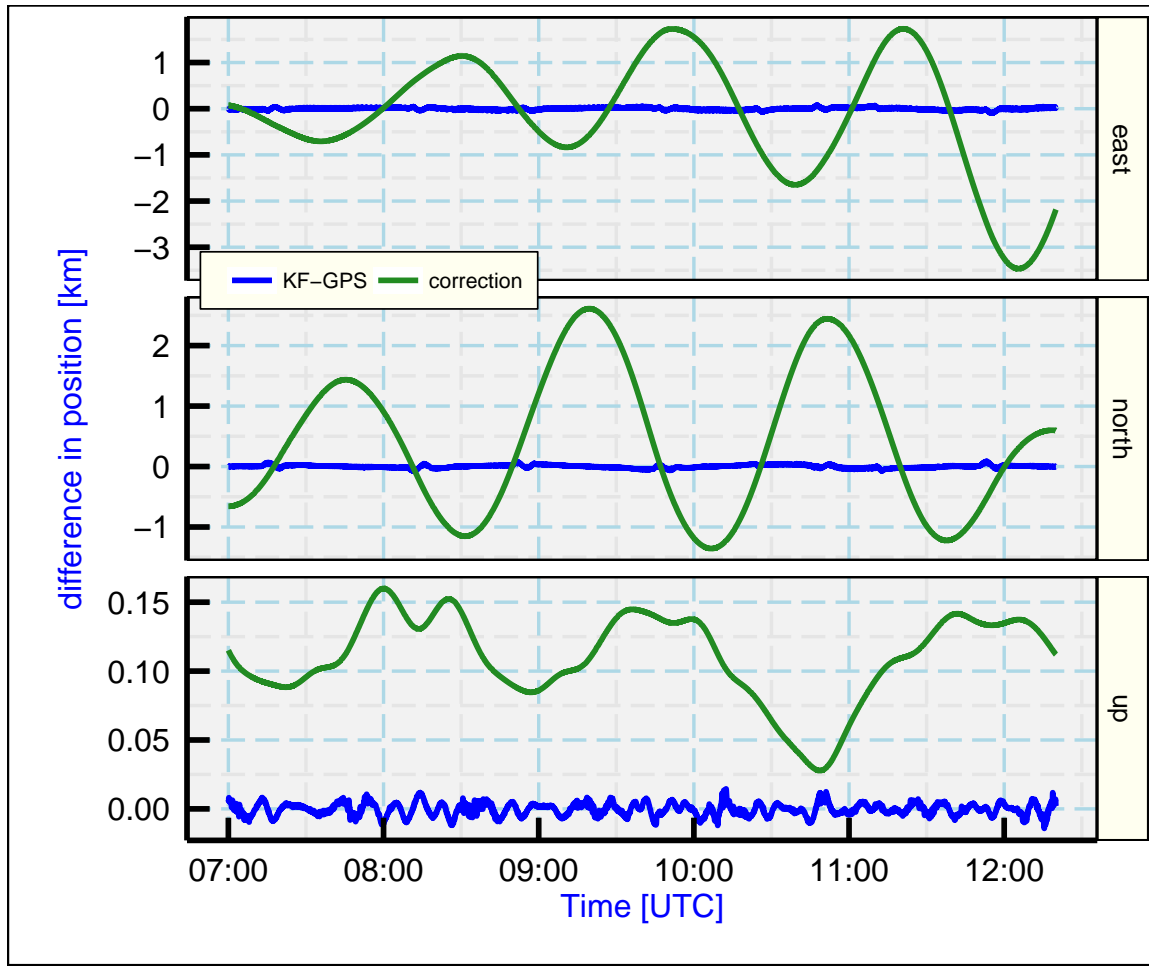


Figure 6: Comparison of the KF (Kalman filter), GPS, and INS values of position for DEEP-WAVE flight 16. DLAT, DLON, and DALT (blue lines) are the differences between the Kalman-filter result and GPS measurement, while CLAT, CLON, and CALT (green lines) are the corrections applied to the original INS values by the Kalman filter.

is negligible ( $< 0.00001$  m/s) and the standard deviation of this difference is about 0.06 m/s, mostly arising in turns and likely the result of small timing differences between INS-provided and GPS-based measurements. There does not appear to be a problem with resolution for the INS variables (VEW and VNS) as there was for position, so no further smoothing of these results is needed. Indeed, plots of the KF and GPS-based variables for short time intervals indicate that there is more noise in the GPS-based variables (GGVEW and GGVNS) than in the KF variables, so using the new variables from the Kalman filter in the calculation of horizontal wind may lead to better high-frequency spectral characteristics than those obtained using the GPS-based variables. This will be explored further in Sect. 5.1. The occasional spikes in this plot are all associated with turns, and they have been minimized by adjustment of the relative timing between the INS-provided and GPS-based variables as well as correction for the rotation rates of the aircraft, but these small residuals remain. Despite some exploration, it has not been possible to reduce them further.

The difference between the KF and GPS-based variables for rate-of-climb of the aircraft, shown in the bottom panel of Fig. 7, needs further explanation. This calculation was first done using the INS-provided variable VSPD as the vertical-motion component of the state variable. While the mean values were similar, the standard deviation in this difference was about 0.28 m/s, which is larger than expected or desirable. The difficulty is attributable to weakness in the INS-provided variable VSPD. Examination of this variable indicates that it has been filtered and shifted in time before being transmitted to the GV data system for recording, and the INS internal processing includes a baro-inertial loop that updates to the pressure altitude. Section 3.1 of this technical note and this memo ([Recommendation161107f.pdf](#)) argue that VSPD is a poor variable to use when calculating the vertical wind and that an alternative variable (ROC) represents the rate of climb of the aircraft better while still remaining independent of the GPS-based measurements. That new variable has been used in the present calculation and in Fig. 7 instead of VSPD. The Kalman filter then updates that variable to the GPS-based measurement (GGVSPD), to produce the new variable ROCKF that is shown in this plot. The mean difference between the GPS value and the corrected measurement from the Kalman filter was -0.001 m/s, with standard deviation 0.11 m/s. Section 5.1.1 explores the characteristics of the new variable (ROCKF) as it would influence calculation of the vertical wind. There it is argued that the level of noise evident in the bottom panel of this plot arises mostly from noise in the GPS-based measurement of rate of climb.

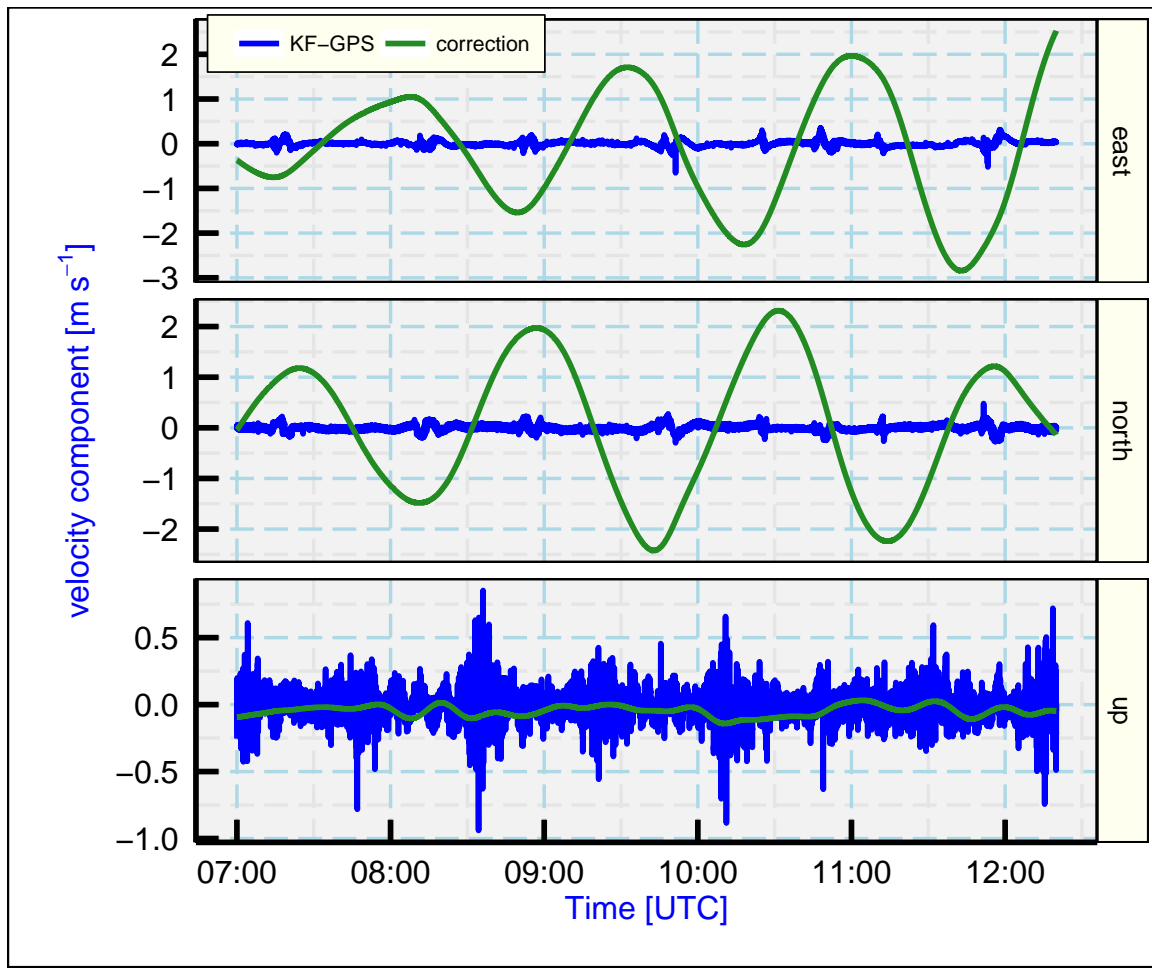
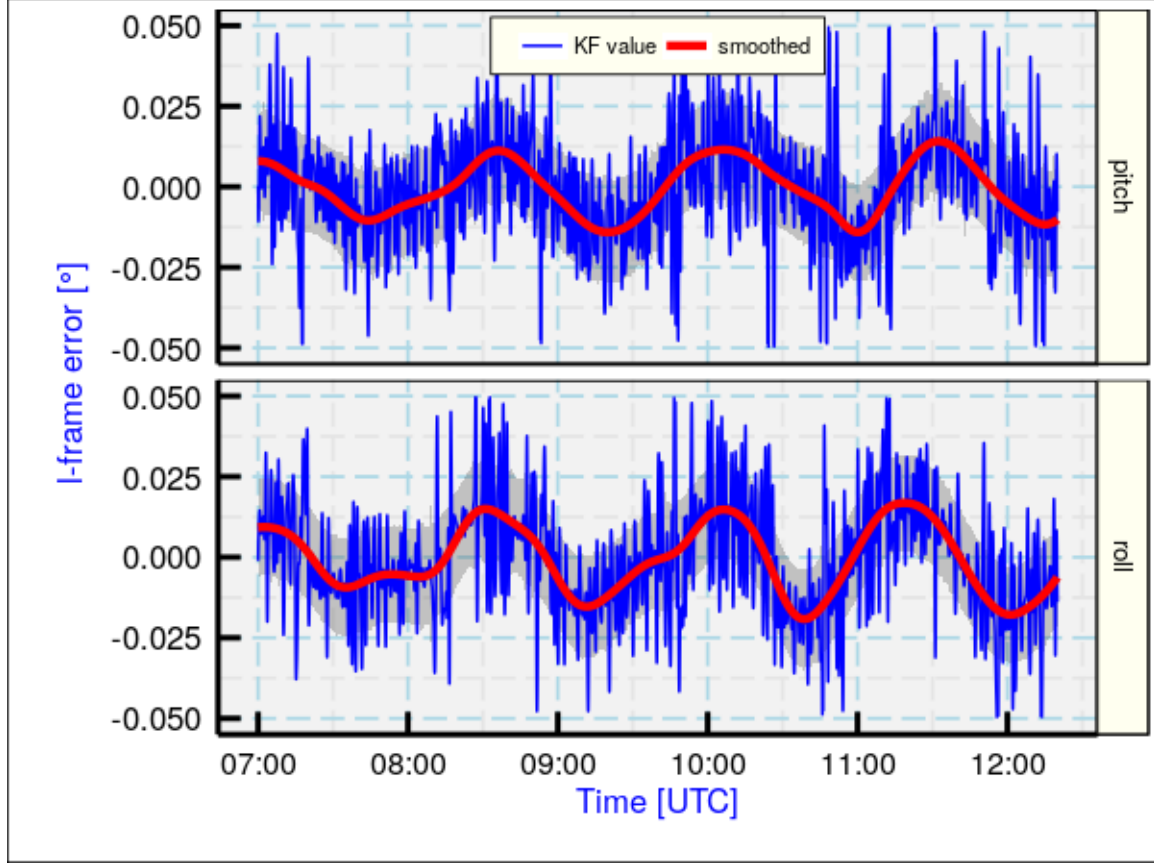


Figure 7: Comparison of the KF, GPS, and INS values of aircraft-velocity components for DEEPWAVE flight 16. Blue lines show the differences between the Kalman-filter results and the corresponding GPS-based values, while the green lines show the corrections applied to the original INS values by the Kalman filter.



*Figure 8: Errors in pitch and roll after transformation to the  $l$ -frame (blue lines). The red lines result from the application of a centered low-pass third-order Butterworth filter to the errors, where the filter cutoff frequency corresponds to a period of 900 s. The shaded ribbon shows the estimated standard uncertainty.*

#### 4.4.3 Roll and pitch

The primary value of this Kalman-filter estimate of error is the improvement in the measurements of attitude angles. Measurements of position and velocity with good quality are already available from the GPS receiver, although some improvement is realized in those cases also. As discussed in Sect. 4.3, it is expected that the errors in pitch and roll will vary more smoothly in the  $l$ -frame than in the  $a$ -frame because each turn changes how any platform misalignment is resolved into errors in pitch and roll. It is therefore useful to transform those errors to the  $l$ -frame for smoothing. The approximate transformation for level flight is

$$\begin{aligned}\delta\theta^{(l)} &= \cos\psi\delta\theta^{(a)} + \sin\psi\delta\phi^{(a)} \\ \delta\phi^{(l)} &= -\sin\psi\delta\theta^{(a)} + \cos\psi\delta\phi^{(a)}\end{aligned}\quad (27)$$

where  $\theta$ ,  $\phi$  and  $\psi$  denote pitch, roll and heading, respectively, and the superscripts in parentheses indicate the reference frame. After this transformation is applied to the error-state vector produced by the Kalman filter, the pitch and roll errors in the  $l$ -frame are as shown in Fig. 8.

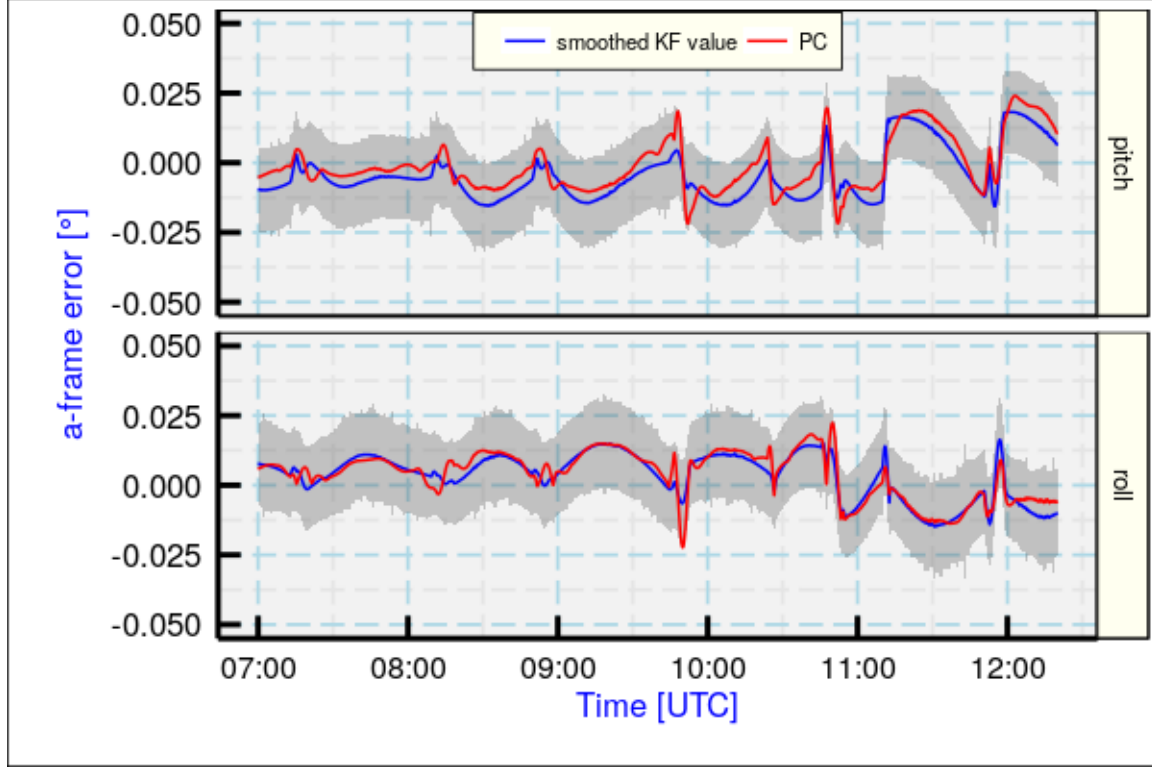


Figure 9: Errors in pitch and roll (blue lines) that result from transforming the filtered result in the previous figure back from the  $l$ -frame to the  $a$ -frame. The red lines show the result of the separate pitch-correction function discussed in the text. The shaded ribbon shows the estimated standard uncertainty in the Kalman-filter result.

As for position and velocity, pronounced Schuler oscillations are evident in both. Also shown in this plot is the result of applying a low-pass third-order Butterworth filter with 900 s cutoff period to the errors. The result is a smoothly varying error signal dominated by the Schuler oscillation that eliminates much of the apparent noise introduced by the Kalman filter. Figure 9 shows the result of transforming the smoothed error signal back to the  $a$ -frame, and it also shows the result of the simplified algorithm of Sect. XX as the red line labeled “PC.” The results from the simplified algorithm are in good agreement with the error estimates from the Kalman filter, with some increased differences in turns as expected. These smoothed errors are then subtracted from the original measurements to obtain corrected results,

The variances associated with  $l$ -frame pitch and roll can be found by appropriate derivation from (27). The resulting variances correspond to a standard deviation of typically about  $0.2^\circ$ , but that then is reduced by an appropriate factor representing the reduction in standard deviation from averaging many points, as was done with the low-pass filter with 900 s cutoff. Averaging 900 points would reduce the expected standard deviation by a factor of  $1/30$ , so this seems an appropriate factor to use when representing the uncertainty in the smoothed correction. The gray ribbon in Fig. 8 shows the resulting standard uncertainty in pitch and roll in the  $l$ -frame, and this then leads to similar standard uncertainty in the  $a$ -frame for the smoothed error estimates, as shown in Fig. 9. The mean standard deviation obtained in this way is  $0.01^\circ$  for both pitch

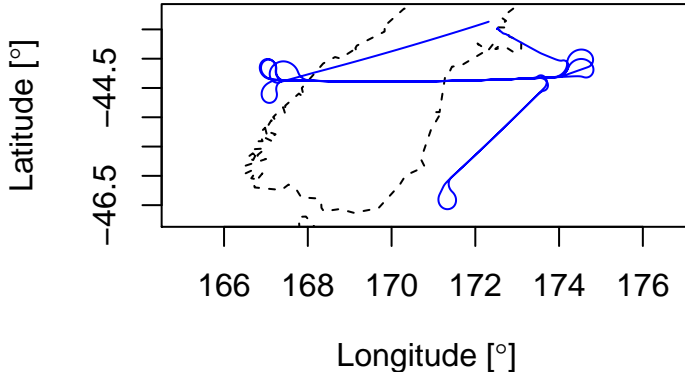


Figure 10: The flight track of about 7 h duration for DEEPWAVE flight 16, 4 July 2012. In the Kalman filter, the many turns provide constraints on the heading. The dashed-line topography shows the South Island of New Zealand.

and roll in either the  $a$ -frame or  $l$ -frame, so this is reasonable estimate of the uncertainty after correction using the Kalman filter.

#### 4.4.4 Heading

The error in heading is more difficult to determine because, for most flight conditions, the heading is poorly constrained and as a result the estimated error in heading often has large uncertainty. The flight path for the particular flight used for this example included frequent changes in flight direction, as shown in Fig. 10, so those turns result in accelerations that can constrain the heading at times spaced throughout during the flight. In Sect. 4.2, it was argued that (15) provides an estimate of the error in heading. However, for the full flight (excluding initial climb and final descent) the mean value provided by this formula was  $0.127^\circ$  but the standard deviation of the correction provided by this equation was  $11.796^\circ$ , so using this correction throughout the flight would introduce unrealistic corrections with large uncertainty. To avoid the noise this would introduce, the estimated error can be considered valid only when horizontal accelerations are large. The top panel in Figure 11 shows the values from (15) for those times when the horizontal acceleration was more than  $1 \text{ m s}^{-2}$ . The mean value of  $\delta\psi$  for these periods was smaller than  $0.001^\circ$  and the standard deviation of the 4295 values was 0.06. This indicates that the uncertainty in the average error in heading is smaller than  $0.01^\circ$  when the average is calculated for the entire flight.

The heading error from the Kalman filter is shown as the blue line in the bottom panel of Fig. 11. The estimate of error usually has large uncertainty as estimated from the covariance estimate from the Kalman filter. As in the top panel, the regions of low uncertainty are confined to the turns where horizontal accelerations are significant. To avoid large corrections with high un-

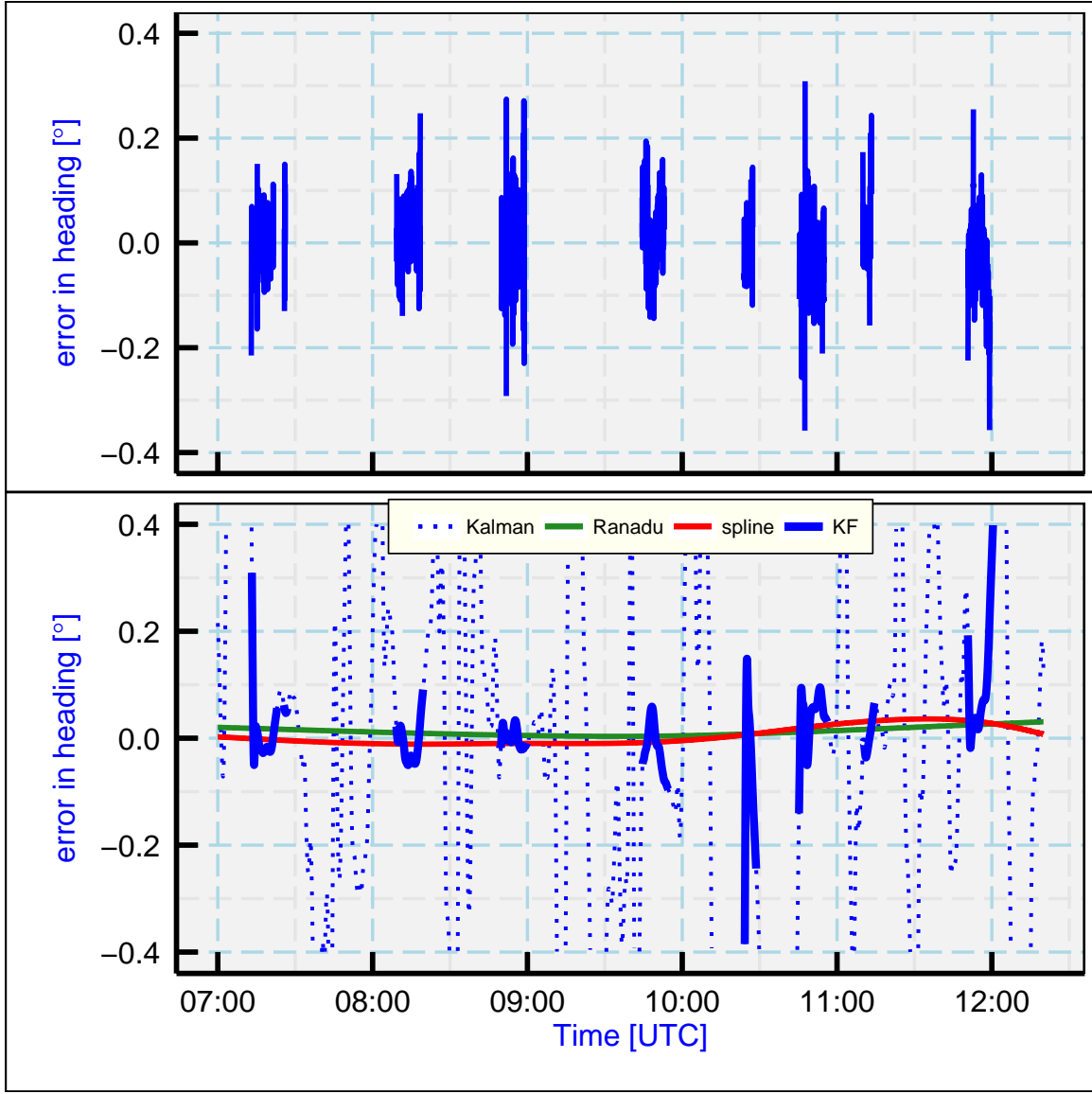


Figure 11: (top) Heading error estimated from (15), for only those periods of DEEPWAVE flight 16 where the horizontal acceleration is larger than  $1 \text{ m s}^{-2}$ . (bottom) Heading correction from the Kalman filter and from Ranadu::CorrectHeading (HC, green line). The results from the Kalman filter are plotted as dotted where the estimated standard deviation exceeds  $0.02^\circ$  and as a thick solid line otherwise. A spline representing the smoothed heading correction from the Kalman filter, using the inverse of the estimated variance as weight factor for the spline, is shown as the red line. Data from DEEPWAVE flight 16.

certainty, a smoothing spline<sup>15</sup> that uses weight factors inversely proportional to the covariance leads to the red line in Fig. 11, for which the mean error is  $< 0.002^\circ$  and the standard deviation for individual measurements is about  $0.02^\circ$ . Another test of the heading error is provided by the correction algorithm “Ranadu::CorrectHeading()” from Sect. 3.3.3, which gives a mean and standard deviation of  $0.005 \pm 0.017$  as shown by the green line in the figure. Perhaps the best interpretation for this flight is that, within about  $0.02^\circ$  uncertainty, there is no heading error. However, in general the spline fit representing the result from the Kalman filter appears to be the preferable correction to the heading.

The results reported by the INS are those that have been used during its internal mechanization to find, for example, the ground-speed components and the *l*-frame accelerations. In processed data sets, it has been common to introduce adjustments to the heading or, less often, the pitch to improve the wind measurements during calibration maneuvers. It is particularly common to find an offset in heading that was introduced to give better agreement for winds during reverse-heading maneuvers. However, it is difficult to separate an offset in sideslip from an offset in heading, as discussed in the NCAR Technical Note on uncertainty in wind measurements. It now appears that the offset often introduced to heading should have instead been an offset in sideslip. Because these offsets are introduced after the INS has performed its internal calculations, the Kalman filter has no mechanism for detecting that an offset has been introduced and will still produce estimates of heading error applicable to the original measurements. It is therefore important to remove any ad hoc adjustments that have been introduced to heading or other INS-provided variables before applying the Kalman filter.

---

<sup>15</sup>The “smooth.spline()” function provided by the “stats” package in R [R Core Team \[2016\]](#) was used, with parameter “spar=1.1” to give strong smoothing.

## 5 New variables for wind

### 5.1 Calculating the wind

#### 5.1.1 The vertical wind

The result of the Kalman filter is that new corrected variables {LATKF, LONKF, ALTKF, VEWKF, VNSKF, ROCKF, PITCHKF, ROLLKF, and THDGKF} are available. These and the variables {TASX, ATTACK, SSLIP} can be used in a new calculation of the vector wind. For the vertical wind, the new variable PITCHKF should be superior to the original variable PITCH and should lead to some improvement. The other critical measurement used to calculate vertical wind is the rate-of-climb of the aircraft, for which there are two options: ROCKF and GGVSPD. The former uses the accelerations from the INS and so should have the best high-frequency characteristics, although GPS receivers provide very good measurements now even at high frequency. The other difference between these two choices is that if GGVSPD is used then a correction is needed for the separation of the GPS antenna from the INS. ROCKF is based on measurements from the INS, with slow updating to the GPS value through the Kalman filter, so it does not need such a correction.<sup>16</sup>

Figure 12 shows a comparison of the variance spectra from the GPS-based value (GGVSPD) and the Kalman-filter value (ROCKF). The spectra are nearly identical, but GGVSPD appears to have some high-frequency noise not present in ROCKF. At these high frequencies, both have contributions to the vertical wind that are insignificant in comparison to that from the relative wind (air motion relative to the aircraft), so it will make little difference which is used in wind calculations, but ROCKF is the preferred choice because high-frequency fluctuations in rate of climb are probably not present.

Variance spectra for the measurements of vertical wind for the same flight segment are shown in Fig. 13. There are small but significant differences, particularly for frequencies around 0.1 Hz where the rate of climb makes an important contribution to the measurement of vertical wind. (At higher frequencies, the relative wind makes the dominating contribution; at lower frequencies, the aircraft is controlled to maintain altitude so again the relative wind is dominant.) A comparison of the two measurements of vertical wind is shown in Fig. 14. While the two represent almost the same signal, the differences at any given time can be significant, as emphasized by the bottom panel in the figure. The standard deviation of the difference between measurements for the interval shown in this figure is 0.12 m/s, so the difference is the same as the claimed uncertainty in measured vertical wind. The evidence from Sect. 4.4.3 indicates that the standard uncertainty in pitch has been reduced from an estimated error of 0.02° to 0.01°. This is the dominant source of error in the measured vertical wind; its inclusion in the uncertainty estimate for vertical wind indicates reduction in the standard uncertainty from about 0.12 m/s to about 0.07 m/s.

<sup>16</sup>An aspect of the corrected vertical wind that needs further investigation is the relative timing of measurements entering the calculation, especially the INS-provided variables PITCH and ACINS as they might be offset from the vertical component of the relative wind as determined from the airspeed (TASX) and angle of attack (AKRD).

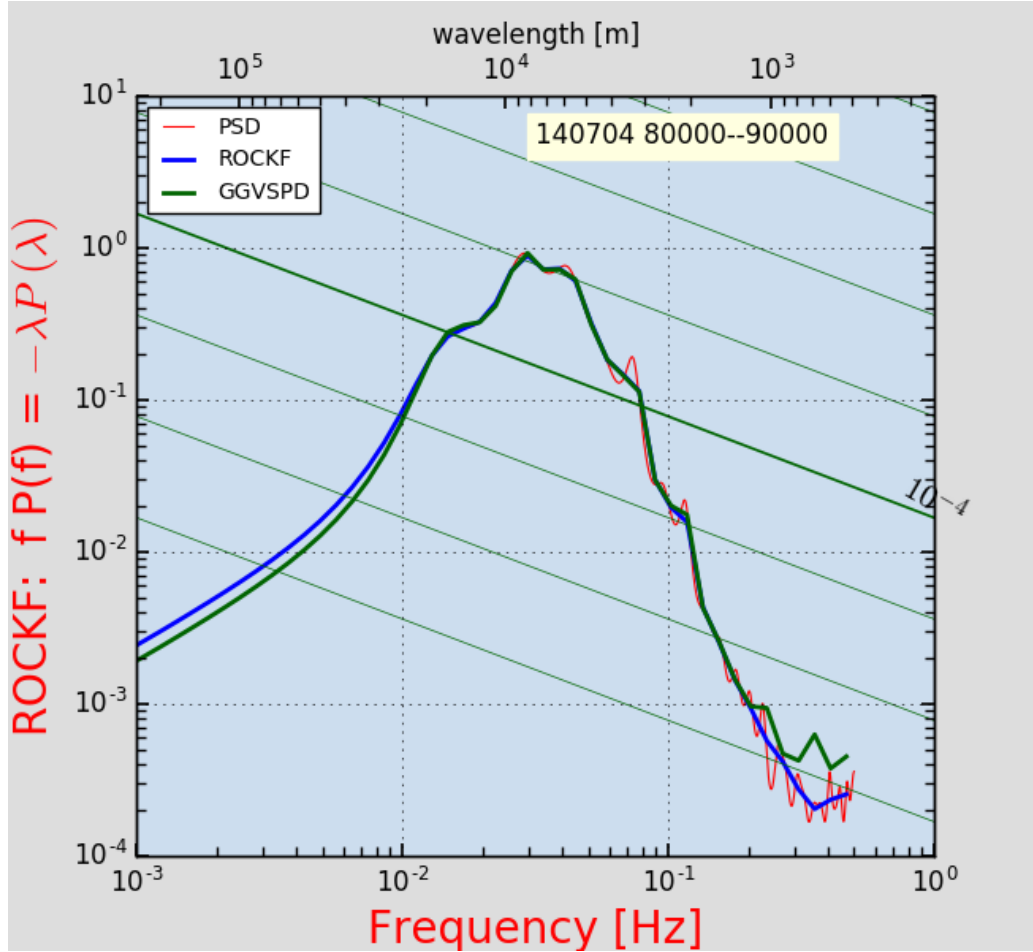


Figure 12: Variance spectra for the rate-of-climb measurements from the GPS receiver (GGVSPD) and the integrated INS-provided acceleration adjusted to match the rate of climb required by the hydrostatic equation (ROCKF). The thin red line shows the spectrum without smoothing for ROCKF; other lines have been smoothed in 50 bins in the logarithm of frequency. Data from a region with intense waves encountered during DEEPWAVE flight 16 on 4 July 2014 over New Zealand.

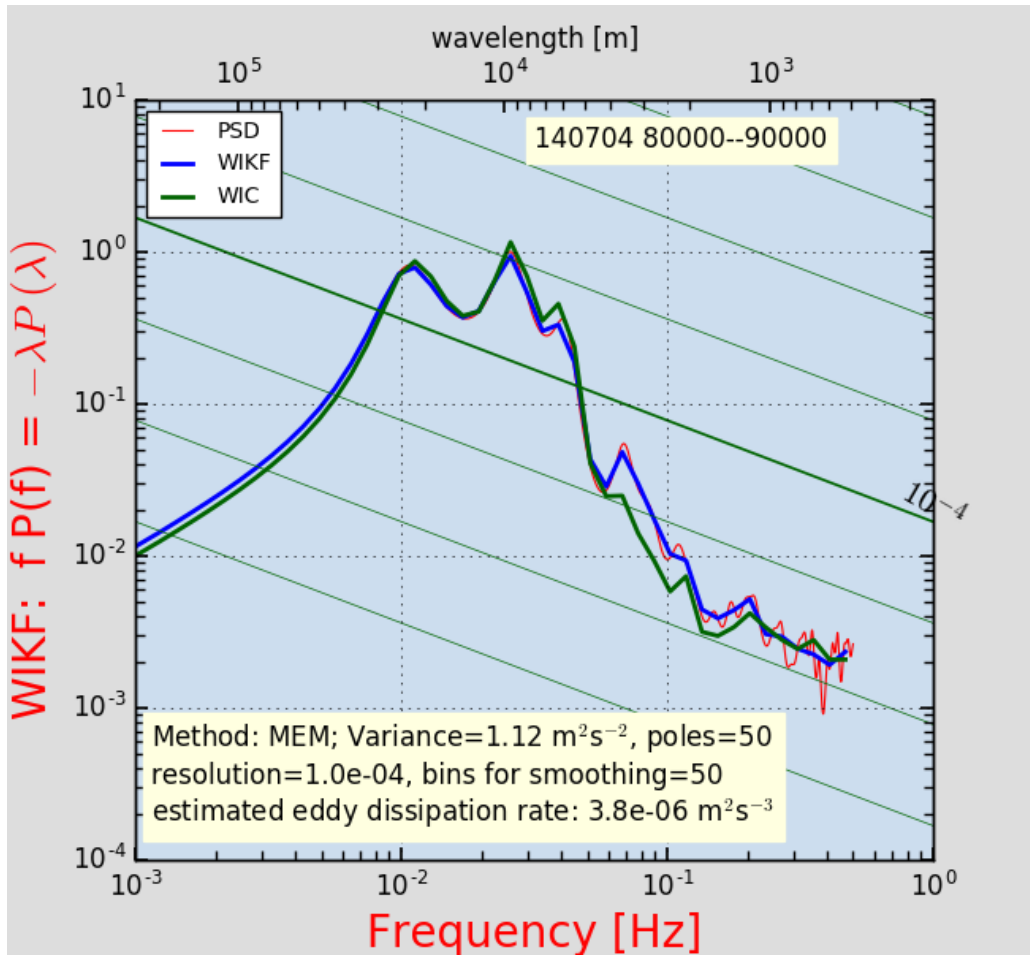


Figure 13: Variance spectra for two measurements of the vertical wind, WIKF as adjusted by the Kalman filter and WIC from conventional data processing. The thin red line shows the spectrum without smoothing for WIKF; other lines have been smoothed in 50 logarithmic frequency bins. Measurements from a region where intense waves were encountered during DEEPWAVE flight 16, 4 July 2014.

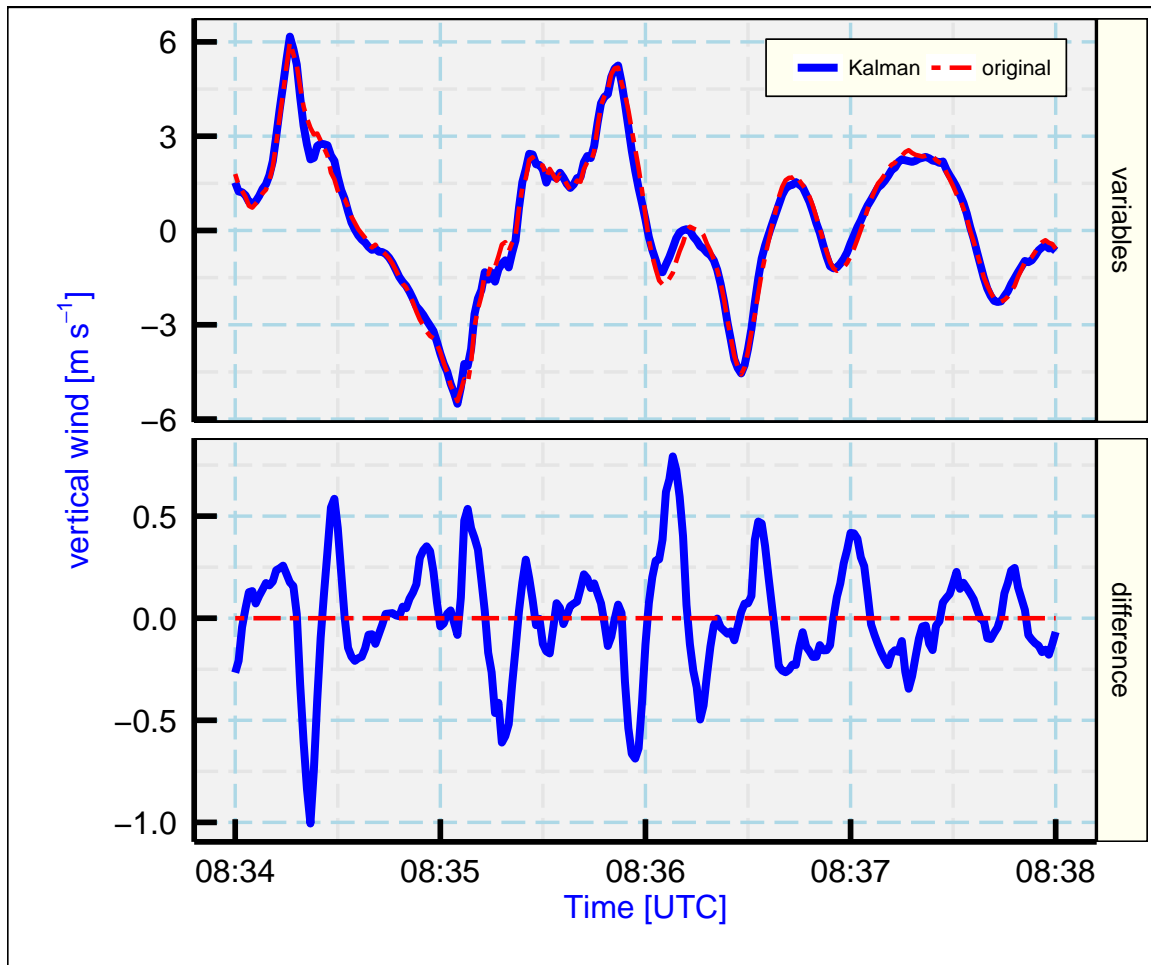


Figure 14: Vertical wind calculated using the results from the Kalman filter, compared to the original calculation before Kalman-filter correction. The difference is shown in the bottom panel. The result labeled "Kalman" is calculated using ROCKF and other results after correction by the Kalman filter, while WIC was calculated using GGVSPD from the GPS for the rate-of-climb of the aircraft. Data from a segment of DEEPWAVE flight 16 where intense waves were encountered.

### 5.1.2 The horizontal wind

The conventional measurements of horizontal wind, provided by the direction WDC and speed WSC, are based on the relative wind added to the ground-speed components VEWC and VNSC. These are adjusted in standard data processing to match the GPS-based measurements via a complementary filter that uses the slowly varying components from the GPS and the faster varying components from the INS ([Cooper et al. \[2016\]](#)). This complementary filter therefore should produce results quite similar to the variables VEWKF and VNSKF from the Kalman filter. For the example flight being used (DEEPWAVE flight 16), the standard deviation of the difference between the corrected measurements and the complementary-filter results is 0.1 m/s and the mean difference is < 0.0001 m/s, so these are in very good agreement. These differences are plotted in Fig. 15. The resulting measurements of horizontal wind direction match with a standard deviation of 0.3° and the magnitudes of the horizontal winds match with a standard deviation of 0.1 m/s. In both variables the differences show a Schuler oscillation. The complementary filter uses a recursive filter that leaves a small residual from the Schuler oscillation, so the corrected result from the Kalman filter is preferable. The plot also shows some larger fluctuations in turns that likely point to residual timing differences among the components entering the calculation of the wind. The difference in heading between the two measurements also would affect the measured horizontal wind, but in this case the heading correction is small and slowly varying so it will have little effect on the results.<sup>17</sup>

Despite these small differences, representative variance spectra for the longitudinal and lateral wind overlap in plots so well that the spectra are indistinguishable. An example is shown in Fig. 16. Nevertheless, Fig. 15 and the standard deviations quoted above indicate that there are significant differences and that the Kalman-filter reduces errors in the horizontal wind by an amount that is significant in comparison to the estimated uncertainty. The reduction in uncertainty arises from the reduced uncertainty in heading, from about 0.10° to about 0.01°, leaving heading as an insignificant source of uncertainty in the lateral component of the horizontal wind and reduces the standard uncertainty from 0.44 m/s to 0.22 m/s, using the elemental contributions to uncertainty in [Cooper et al. \[2016\]](#), Table 8 and the summary in that reference on p. 51. The remaining uncertainty is now dominated by the uncertainty in measurement of sideslip, and recent studies of the sideslip using a laser air-motion sensor suggest that there is still opportunity to improve that measurement also.

## 5.2 Adding the new variables to the netCDF file

The code shown in the box that follows adds one variable to an existing netCDF file, renaming the resulting file with a name like PROJECTrf01KF.nc if the original file was PROJECTrf01.nc. This can serve as a model for adding such variables. See the “.Rnw” file for the actual code, which has additional statements to protect against missing variables or substitute variables when

---

<sup>17</sup>The heading-change correction needed to account for the separation between the INS and GPS antenna has little effect on the horizontal wind because both the Kalman filter and the complementary filter smooth any short-term contributions to the GPS-based measurements. For completeness, however, the GPS-based measurements GGVEW and GGVNS have been corrected for the effect of heading change before use in the Kalman filter or the complementary filter.

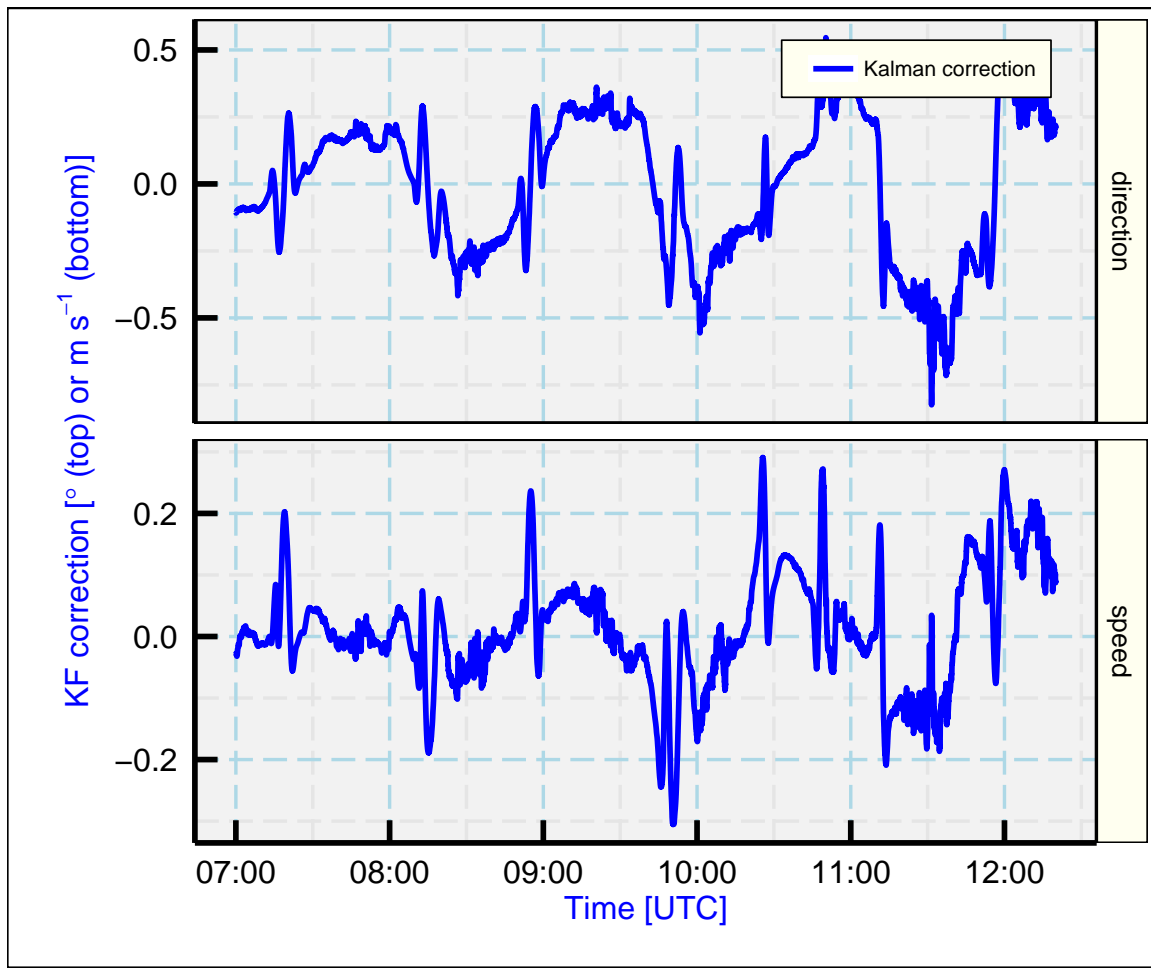


Figure 15: Differences between the conventional measurements of horizontal wind (variables WDC and WSC) and the results from the Kalman filter (variables WDKF and WSKF).

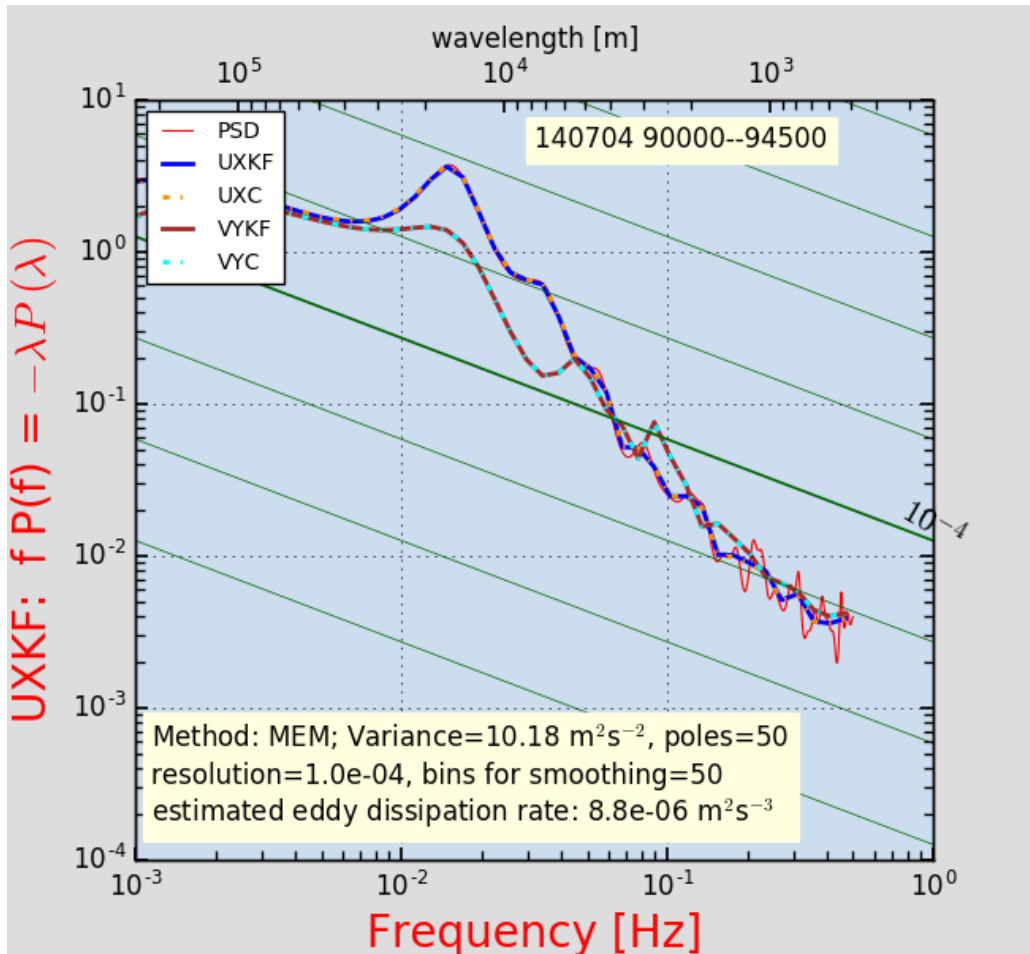


Figure 16: Variance spectra for the standard variables UXC and VYC, which are measurements of the longitudinal and lateral components of the horizontal wind relative to the orientation of the aircraft, and the corresponding results for the winds produced after correction by the Kalman filter (UXKF and VYKF). The thin red line shows the spectrum without smoothing for UXKF; the other lines have been smoothed in 50 logarithmic bins in frequency. Data are from DEEPWAVE flight 16, 4 July 2014, in waves over New Zealand.

some are missing and to handle high-rate data files. This example is included to serve as a template for other scripts that might want to add variables to a netCDF file. The processing script “KalmanFilter.R” adds these variables in a similar way: LATKF, LONKF, ALTKF, VEWKF, VNSKF, ROCKF, PITCHKF, ROLLKF, THDGKF, WDKF, WSKF, WIKF, WICC, WDCC, WSCC, UXKF, VYKF. All ending in KF are the same as the original name without KF but after applying the correction from the Kalman filter. Three other variables ending in CC are those calculated in the standard way but with measurements from the GPS receiver corrected for the rotation of the aircraft, which was not included in the original processing. The table of variable names at the end of this technical note includes definitions for these and the other netCDF variables that have been used.

**Example of code to add a variable:**

```

## get the old netCDF variables:
D <- getNetCDF (fname, VarList)
## open the copy of the old file for writing:
netCDFfile <- nc_open (fnew, write=TRUE)
Rate <- 1 ## the data rate of this file
## retrieve dimension info from the old file
Dimensions <- attr (D, "Dimensions")
Dim <- Dimensions[["Time"]]
## variables to add to the netCDF file: (add more)
VarNew <- c("LATKF")
VarOld <- c("LAT")
VarUnits <- c("degrees")
VarLongName <- c("latitude, KF")
VarStdName <- c("INS latitude, Kalman-filter-corrected")
## create the new variables
varCDF <- list ()
for (i in 1:length(VarNew)) { ## only one in this example
  ## create the new variable and add it to the netCDF file
  varCDF[[i]] <- ncvar_def (VarNew[i],
                            units=VarUnits[i],
                            dim=Dim,
                            missval=as.single(-32767.), prec="float",
                            longname=VarLongName[i])
  if (i == 1) {
    newfile <- ncvar_add (netCDFfile, varCDF[[i]])
  } else {
    newfile <- ncvar_add (newfile, varCDF[[i]])
  }
  ## transfer attributes from the old variable and add new ones
  ATV <- ncatt_get (netCDFfile, VarOld[i])
  copy_attributes (ATV, VarNew[i], newfile)
  ncatt_put (newfile, VarNew[i], attname="standard_name",
             attval=VarStdName[i])
  ## add the measurements for the new variable
  ncvar_put (newfile, varCDF[[i]], D1[, VarNew[i]])
}
## then close to write the new file
nc_close (newfile)

```

## **6 Summary and conclusions**

An application of an error-state Kalman filter has been developed to improve the measurements of wind provided by the NSF/NCAR GV research aircraft. The primary advantage provided by the corrected measurements is reduction in the uncertainty associated with the measurements of pitch and heading, which without correction are the largest sources of uncertainty in the measurements. The corrected measurements reduce the standard uncertainty in measured vertical wind and the lateral component of the horizontal wind to about 50% of their previous values, to about 0.07 and 0.22 m s<sup>-1</sup>. The Kalman filter has a much smaller effect on the longitudinal component of the horizontal wind because that uncertainty is determined mostly by elemental contributions from the measurement of airspeed and temperature, which are not affected by the Kalman filter, and only to a small extent by the ground speed which is measured well by GPS without the Kalman filter. The program that implements this procedure for correction of the measurements can be used with data archives from past projects as long as the measurements in those archived files include the aircraft velocity from INS and GPS sources and the INS-based attitude angles.

## A Appendix: Reproducibility

This document is constructed in ways that support duplication of the study. The code that generates the plots and implements the Kalman filter is incorporated into the same file that generated this document via L<sup>A</sup>T<sub>E</sub>X, using principles and techniques described by Xie [2013] as implemented in the R package 'knitr' (Xie [2014]). The program, 'KalmanFilterTechNote.Rnw', is archived on 'GitHub' in the directory at [this URL](#). There is some supplemental material in that directory, including the workflow document, the bibliography and many code segments saved in the "chunks" subdirectory, so the full directory should be downloaded in order to run the program. The calculations use the programming language R (R Core Team [2016]) and were run within RStudio (RStudio [2009]), so this is the most straightforward way to replicate the calculations and the generation of this document.

A package named Ranadu, containing auxillary functions, is used extensively in the R code. It is available on GitHub as <https://github.com/WilliamCooper/Ranadu.git>. The version used for calculations in this technical note is included in the 'zip' archive listed below.

The data files used are also preserved in the NCAR High Performance Storage System (HPSS) in files that are available, and they can be provided via a request to <mailto:raf-dm@eol.ucar.edu>. The original files containing the data as produced by the NCAR Earth Observing Laboratory, Research Aviation Facility, were in netCDF format (cf. [this URL](#)), but in many cases data archives were reprocessed and the files may change after reprocessing so a separate archive is maintained for this document. The data files in this archive contain R data.frames and are preserved as binary-format 'Rdata' files via R 'save' commands. The code in the GitHub archive has appropriate 'load' commands to read these data files from a subdirectory named 'Data' (/Data or ~/Data or /home/Data) but this is not part of the GitHub repository because it is too large to be appropriate there. To reproduce this research, those data files have to be transferred separately from the NCAR HPSS to the 'Data' directory.

Extensive use has been made of attributes assigned to the data.frames and the variables in those data.frames. All the attributes from the original netCDF files have been transferred, so there is a record of how the original data were processed, for example recording calibration coefficients and processing chains for the variables. Once the data.frames are loaded into R, these attributes can be viewed and provide additional documentation of what data were used. Key information like the processing date, the program version that produced the archive, and the selection of primary variables for various measurements thus is preserved.

PROJECT:	KalmanFilterTechNote
ARCHIVE PACKAGE:	KalmanFilterTechNote.zip
CONTAINS:	attachment list below
PROGRAM:	KalmanFilterTechNote.Rnw
ORIGINAL DATA:	/scr/raf_data/DEEPWAVE/
GIT:	<a href="https://github.com/WilliamCooper/KalmanFilterTechNote.git">https://github.com/WilliamCooper/KalmanFilterTechNote.git</a>

## References

- W. A. Cooper, R. B. Friesen, M. Hayman, J. B. Jensen, D. H. Lenschow, P. A. Romashkin, A. J. Schanot, S. M. Spuler, J. L. Stith, and C. Wolff. Characterization of uncertainty in measurements of wind from the NSF/NCAR Gulfstream V research aircraft. proposed NCAR technical note, undergoing review NCAR/TN-XXX+STR, Earth Observing Laboratory, NCAR, Boulder, CO, USA, jan 2016. URL <https://drive.google.com/open?id=0B1kIUH45ca5AT2NwVFpqRFN0ZOU>. 1.1, 3.3.1, 3.3.2, 3.4, 4.2, 5.1.2
- Paul Gilbert and Ravi Varadhan. *numDeriv: Accurate Numerical Derivatives*, 2016. URL <https://CRAN.R-project.org/package=numDeriv>. R package version 2016.8-1. (document)
- D. H. Lenschow and P. Spyers-Duran. Measurement techniques: air motion sensing. Technical report, National Center for Atmospheric Research, 1989. URL <https://www.eol.ucar.edu/raf/Bulletins/bulletin23.html>. 2, 3.3.3
- A. Noureldin, T.B. Karamat, and J. Georgy. *Fundamentals of Inertial Navigation, Satellite-based Positioning and their Integration*. SpringerLink : Bücher. Springer Berlin Heidelberg, 2013. ISBN 978-3-642-30465-1. doi: 10.1007/978-3-642-30466-8. URL <https://books.google.com/books?id=qGbsW6sDr7YC>. 1, 2, 3, 3.2.1
- R Core Team. *R: A language and environment for statistical computing*. R Foundation for Statistical Computing, Vienna, Austria, 2016. URL <http://www.R-project.org>. (document), 15, A
- RStudio. *RStudio: Integrated development environment for R (Version 0.98.879)*, 2009. URL <http://www.rstudio.org>. (document), A
- M. Schuler. The perturbation of pendulum and gyroscope instruments by acceleration of the vehicle. *Physik. Z.*, 24(16):344–357, 1923. URL <http://www.webcitation.org/6JBR8WNRq>. 3.3.2
- H. Wickham. *ggplot2: elegant graphics for data analysis*. Springer New York, 2009. ISBN 978-0-387-98140-6. URL <http://had.co.nz/ggplot2/book>. (document)
- Y. Xie. *Dynamic Documents with R and knitr*. Chapman and Hall/CRC, Boca Raton, Florida, 2013. URL <http://yihui.name/knitr/>. ISBN 978-1482203530. (document), A
- Y. Xie. *knitr: A general-purpose package for dynamic report generation in R*, 2014. URL <http://yihui.name/knitr/>. R package version 1.6. (document), A

# Variable Names and Acronyms

ACINS: vertical acceleration, INS, 15, 43	VEW: ground speed eastward, INS, 7, 18, 21, 36
AKRD: angle of attack, radome, 43	VEWC: ground speed eastward, GPS corrected, 43
ALT: altitude, INS, 15, 34	VEWKF: ground speed eastward, Kalman filter, 43, 47
ALTKF: altitude, Kalman filter, 43, 47	VNS: ground speed northward, INS, 7, 18, 21, 36
ATTACK, <i>see also</i> AKRD	VNSC: ground speed northward, GPS corrected, 43
BLATA: body-lateral acceleration, 7, 8	VNSKF: ground speed northward, Kalman filter, 43, 47
BLONGA: body-longitudinal acceleration, 7, 8	VSPD: rate of climb, INS, 7, 15, 17, 18, 36
BNORMA: body-normal acceleration, 7, 8	VYC: lateral wind, GPS corrected, 47
BYAWR: body yaw rate, inertial, 10	VYKF: lateral wind, Kalman filter, 47
GGALT: altitude, GPS, MSL, 21	WDC: wind direction, GPS corrected, 43
GGLAT: latitude, GPS, 34	WDCC: WDC recalculated, 47
GGLON: longitude, GPS, 34	WDKF: wind direction, Kalman filter, 47
GGIEW: ground speed eastward, GPS, 21, 32, 47	WIC: vertical wind, GPS corrected, 43
GGVNS: ground speed northward, GPS, 21, 32, 47	WICC: WIC recalculated, 47
GGVSPD: rate of climb, GPS, 15, 17, 43	WIKF: vertical wind, Kalman filter, 43, 47
LAT: latitude, INS, 21, 34	WSC: wind speed, GPS corrected, 43
LATC: latitude, GPS-corrected, 21	WSCC: WSC recalculated, 47
LATKF: latitude, Kalman filter, 43, 47	WSKF: wind speed, Kalman filter, 47
LON: longitude, INS, 34	ZROC: altitude, INS new, 34
LONKF: longitude, Kalman filter, 43, 47	
PITCH: pitch angle, INS, 21, 43	
PITCHKF: pitch angle, Kalman filter, 43, 47	
ROC: rate of climb, INS new, 15, 17, 36	
ROCKF: rate of climb, Kalman filter, 36, 43, 47	
ROLL: roll angle, INS, 21	
ROLLKF: roll angle, Kalman filter, 43, 47	
SSLIP: sideslip, radome, 43	
TASX: airspeed, relative wind, 43	
THDG: heading, INS, 21	
THDGKF: heading, Kalman filter, 43, 47	
UXC: longitudinal wind, GPS corrected, 47	
UXKF: longitudinal wind, Kalman filter, 47	

# Index

- a-frame, *see* reference frame, a-frame
- acceleration
  - a-frame, 8, 24
  - Coriolis, *see* inertial corrections
  - determined from GPS, 22
  - fits, 8
  - from GPS, 22, 24
  - from velocity derivative, 8
  - gravity, *see* gravity
  - horizontal
    - needed magnitude, 23
    - required magnitude, 23, 24, 32, 40
  - l-frame, 8, 18, 24, 30, 42
  - lag, 24, 31
  - lateral, 8, 10, 27
  - measurement, 1–3, 5–8, 10, 17, 18, 20–22, 27, 28, 30, 31, 43
  - normal component, 6
  - retrieving, 18, 22
  - smoothing, 30
  - vertical, 44
- accelerometer
  - bias, 20, 27, 29
  - calibration, *see* calibration, accelerometer
  - error, 21, 29
  - noise, 28, 29
- aircraft
  - coordinate system, 6
  - instrumentation
    - GPS, 1
    - INS, 1
    - IRU, 1
  - NSF/NCAR GV, 1, 2, 10, 11, 20, 22, 25, 26, 29, 36, 51, 53
- airspeed, 10, 11, 25, 31, 43
- algorithm
  - correct heading, 2
  - correct pitch, 2
  - Kalman filter, 27
  - search for turns, 24
  - simplier
    - correct heading, 18, 21, 23, 42
- correct pitch, 18, 21
- Ranadu reference, 24
- wind, 1
- alignment
  - INS, 1
- altitude of aircraft, 5, 6, 27
  - geometric, 2, 15, 34
- Kalman filter, 34
- new variable ZROC, 34
- pressure, 2, 15, 34, 36
- angle of attack, 43
  - empirical representation, 2, 25
  - new approach, 25
  - reference for calibration, 25
  - standard reference, 25
- angle, attitude, *see* attitude angle
- archive
  - for this document, 30, 52
  - data, 52
- attack, *see* angle of attack
- attitude angle, 1–3, 5, 6, 17, 21, 30, 38
  - correction, 3
  - definition, 22
  - derivative, 5, 7, 10, 17, 18
  - errors, 3, 18
  - lag, 8, 30
  - new mechanization, 11
- attributes
  - data.frame, 52
  - variable, 52
- baro-inertial loop, 36
- body acceleration, *see* acceleration
- body rotation rate
  - see rotation rate of aircraft, 1
- calibration
  - accelerometer, 7, 8, 10, 18, 20
  - fit coefficients, 8
  - coefficients
    - used in processing, 52
- rotation rate, 10

comparison  
 acceleration, 10  
 altitude, 2  
 heading rate of change, 11  
 independent INS units, 31  
 INS to GPS, 3, 18, 21  
 plot  
   attitude angles, 11  
   Kalman filter results, 34, 36  
   rate of climb, 17  
   rotation rate, 18  
   velocity components, 11  
 rotation rate, 10  
 to INS mechanization, 11  
 Coriolis, *see* inertial corrections  
 correction  
   for aircraft rotation, 29, 36  
 coupling  
   strong, 1, 3, 20, 30, 32  
   weak, 23  
 covariance, *see* matrix, covariance  
 data  
   new archive, 2  
   requesting, 52  
   standard archive, 2, 3, 11, 17, 18, 25, 30  
 data processing  
   conventional, 45  
 data rate, 34  
 DEEPWAVE research project, 7, 10, 11, 18, 25, 30, 31, 34, 36, 40, 43–45, 47, 49, 52, 53  
   full name, 7  
 derivations  
   in workflow, 2  
 derivative  
   --, *see* --, derivative  
   Savitzky-Golay, 22  
   state vector, *see* state vector, derivative  
   transformation to a-frame, 10  
 derivative function, 4, *see* function, derivative  
 deviation, standard  
   acceleration, 7  
   difference in wind, 47  
   fit residual, 8

heading correction, 24, 40, 42  
 heading error, 31, 32  
 measurements, 28  
 pitch correction, 39  
 position difference, 34  
 turn rate, 11  
 velocity difference, 34, 36, 43

Earth  
   radius, *see* radius of curvature  
   reference frame, 5  
   rotation rate, 6, 7, 22  
 error  
   acceleration, 27  
   effect of, 21  
   strong coupling, 20  
 accelerometer, 20, 21, 29  
 attitude angle, 2, 3  
   Kalman filter estimate, 18  
 complementary filter, 47  
 estimate from Kalman filter, 2  
 heading, 1, 2, 18, 21, 23, 30, 32, 40  
   additional constraint, 31  
   comparison of INSs, 31  
   correction, 40  
   effect of imposed offset, 42  
   effect of lag, 23, 24, 31  
   effect on pitch, 21  
   equation for, 22  
   estimate, 22, 24, 29, 32  
   mean, 32  
   need for turns, 31  
   spline fit, 40  
   uncertainty, 40  
 horizontal acceleration, 20  
*l*-frame, 5  
 measured INS-GPS, 4  
 mix pitch and roll, 20  
 pitch, 1, 2, 5, 20  
   a-frame, 21, 39  
   dependence on noise, 29  
   estimation, 20  
   Kalman-filter result, 38  
*l*-frame, 21  
 Ranadu, 21

- smoothed, 39
- strong coupling, 20
- uncertainty, 39
- position, 18
  - strong coupling, 20
- roll, 5, 20, 29
  - a-frame, 21
  - l-frame, 21
  - Ranadu, 21
- rotation rate, 27
- smoothing, 30, 32
  - l-frame, 33
- state vector, *see* state vector, error in timing, 23, 31
- velocity, 18, 20, 21
  - wind, effect of Kalman filter, 47
- error-measurement vector, 32
- error-state vector, 3–5, 27, 29, 30, 38
  - propagation, 27
- file
  - data, 2, 3, 11, 17, 30, 32, 47, 52
    - archive, 52
    - variable, *see* netCDF Variable Names
  - netCDF, 47, 52
- filter
  - Butterworth, 15, 25, 34, 39
  - centered, 47
  - complementary, 47
  - cutoff frequency, 15, 34, 38, 39
  - Kalman, *see* Kalman filter
  - low pass, 15
  - phase-shift, 15
  - recursive, 47
  - Savitzky-Golay, 7, 24
- fit
  - angle of attack, 25
    - new, 25
  - coefficients
    - rotation rate, 11
  - regression
    - acceleration, 8
    - rotation rate, 11
  - time shift, 31
- flight path
- recommendation, 23, 32
- flight segments
  - for heading correction, 24
- function
  - Butterworth filter, 15
  - CorrectPitch, 21, 39
  - derivative, 4, 11, 14, 27, 28
    - extension, 27
  - HeadingCorrection, 24
  - Jacobian, 28, 53
  - producing the derivative vector, 3
  - Ranadu, 52
  - ShiftInTime, 32
  - spline, 40
- gas constant, 15
- ggplot2, 53
- GitHub repository, 21, 24, 52
- global positioning system, *see* navigation system, GPS
- GPS, *see* navigation system, GPS
- gravity, 6, 10, 15, 20
- ground speed, 1, 11, 18, 20–24, 34, 42, 43
- gyro, 10, 21
  - bias, 21, 27
- heading, 1, 23
  - correction, 23, 31
    - requirements, 23
    - simplified, 21
    - uncertainty, 31, 32, 40, 42
  - error, 18, 20, 30, 31
    - estimate from acceleration, 30
    - reference, 30
  - imposed offset, 42
  - Kalman filter results, 40
  - rate of change, 10, 11
  - weak coupling, 30
- heading\*\*, 5, 6, 43
- HPSS archives, 52
- hydrostatic equation, 15
- inertial corrections, 6, 7, 10, 11, 17, 18, 31
- inertial reference unit, 1–7, 10, 17, 30
  - bias, 21
- surrogate for measurement, 2

- INS, *see* navigation system, inertial instructions  
 R script, 2, 30
- integration  
 duplicating INS, 11  
 INS, 29  
 altitude, 15  
 rate of climb, 15  
 position error, 20
- interpolation, 15  
 for time shift, 32  
 Kalman-filter results, 34  
 spline, 24
- inversion  
 computational singularity, 28
- IRU, *see* inertial reference unit
- Jacobian  
 numerical evaluation, 28, 53  
 of derivative function, 3, 4, 27, 28
- Kalman filter, 5, 14, 17, 27, 32, 36  
 algorithm, 27  
 coding, 2  
 corrected variable, 34  
 error-state, 1–3, 27, 51  
 matrices, 3, 27–29  
 primary value, 1, 51  
 processing script, 2  
 results  
   heading, 40  
   new variables, 43  
   pitch, 38  
   position, 34  
   roll, 38  
   velocity, 34  
   summary, 3  
   time step, 34  
   uncertainty, 34, 39
- Kalman-gain matrix, 4
- knitr, 52, 53
- l*-frame, *see* reference frame, *l*-frame
- LaTeX, 2
- latitude, 5, 6, 21, 27, 34  
 Kalman filter, 50
- symbol, 6  
 uncertainty, 34
- longitude, 5, 6, 27, 34  
 symbol, 6
- Mach number, 25
- maneuver, 10  
 calibration, 42  
 circle, 10, 11, 23  
 pitch, 7, 10  
 recommended, 23  
 reverse heading, 23, 42  
 speed run, 10, 11  
 yaw, 10, 11
- matrix  
 coordinate  
   transformation, 6  
 coordinate transformation, 5–7, 17, 18  
   derivative, 7, 17  
 covariance, 3, 27, 29, 30, 34
- Kalman gain, 4, 29  
 measurement noise, 4, 29  
 measurement noise covariance, 29  
 noise, 4, 27, 28  
   expansion of, 32  
 noise covariance, 28, 29  
 observation, 4  
   added row, 32  
 skew-symmetric, 17  
 state transition, 3, 4, 27
- measurement  
 acceleration, 2, 3, 6  
   from GPS, 22  
   *l*-frame, 6  
   surrogate, 22
- altitude  
 new, 15  
 offset, 34
- ambient pressure, 25
- attitude angles, 38  
 corrected, 2, 3
- correction  
 caution re use, 42  
 differentiated, 21  
 dynamic pressure, 25

- error
  - Schuler oscillation, 20
  - estimated error, 3
  - from GPS, 1, 3, 4, 8, 18, 20, 27, 30, 31, 36, 38
  - correction to, 47
  - noise, 29, 36
  - uncertainty, 20, 22, 27
  - from INS, 1, 3, 4, 8, 17, 18, 27, 30
  - new rate of climb, 15
  - noise, 28
  - uncertainty, 20
  - VSPD, 17
  - from IRU, 1, 3–5, 7, 10, 11, 17, 21, 22
  - calibration, 8, 10, 11
  - normal acceleration, 6
  - retrieval, *see* measurement, from IRU, surrogate
  - surrogate, 17, 18
  - surrogate for, 2, 10
- from Kalman filter, 39
- heading, 1, 30
  - estimated error, 32
  - offset, 42
  - uncertainty, 23, 42
- IRU
  - surrogate, 17
- lag, 7
- noise in, 4
- pitch, 1, 2, 21
  - corrected, 21
  - error, 20
- position
  - Kalman filter, 34
  - smoothing, 34
  - uncertainty, 34
- pressure, 15
  - uncertainty, 15
- pressure difference
  - radome, 25
- rate of climb, 2, 43
  - Kalman filter, 36
  - variance spectrum, 44
- required by CorrectPitch, 21
- rotation rate, 2, 3, 5
- l*-frame, 7
- offset, 10
- retrieval, 18
- surrogate, 17
- validating, 10
- time lag, 23, 31, 32
- timing, 7
- used in Kalman filter, 29
- velocity, 1
  - correction to, 30
  - Kalman filter, 34
- vertical wind
  - variance spectrum, 43, 45
- wind, 1, 2, 11, 47
  - conventional, 43, 47
  - Kalman filter, 43, 47
  - recommendation, 23, 32
  - variance spectrum, 47
- measurements
  - acceleration, 20
  - error, 20
  - differentiated, 18, 24, 31
  - rate of climb, 25
- mechanization, 1, 3–5, 11, 42
  - definition, 3
  - outline, 5
- navigation system
  - GPS, 1, 3, 4, 7, 8, 10, 11, 15, 17, 18, 20–23, 27, 29–31, 34, 36, 38, 43, 44, 47
  - inertial, 1, 3, 4, 7, 8, 11, 15, 18, 20–22, 24, 27–29, 31, 34, 36, 42, 43
  - alignment, 20
  - mechanization, 3, 5, 10
  - rate of climb, 2
  - timing, 23
  - strap-down, 22
- navigation system, GPS
  - antenna location, 29, 43, 47
- netCDF, 2, 25
  - create new file, 2
- netCDF file, 47
- netCDF format, 52
- netCDF variable
  - model for new, 47

- noise, 3
  - from Kalman filter
  - reducing, 32
  - in heading correction, 40
  - measurement, 4
- NSF/NCAR GV, 1
- OmniSTAR corrections, 29
- overview
  - Kalman filter, 3
  - Kalman filter algorithm, 27
  - this document, 1
- package
  - R
    - Ranadu, 21, 24
    - stats, 40
- pitch
  - correction
    - simplified, 21
  - smoothing
    - l-frame, 38
  - uncertainty
    - a-frame, 39
    - l-frame, 39
  - variance
    - l-frame, 39
- PitchCorrection.R, 21
- pitch\*\*, 5, 6, 43
- platform
  - misalignment, 33, 38
- polynomial
  - Savitzky-Golay, 7, 22, 24
- position
  - derivative, 6
- pressure
  - ambient, 25
  - dynamic, 25
  - static, 25
- processing from archives, 2, 18
- program
  - file, 2, 47, 52
  - for calculations, 2
  - generating this document, 52
  - interactive, 30
- language
  - R, 2
  - R language, 52
- program file, 2
- program for calculation
  - R language
    - chunk, 30, 52
- R
  - data.frames, 52
  - RStudio, 52
- R language, 2, 52
- R package
  - ggplot2, 53
  - knitr, 52
  - numDeriv, 53
  - Ranadu, 52
- radius of curvature
  - Earth, 20, 27
  - meridional, 6
  - normal, 6
- radome
  - pressure ports, 25
- Ranadu, 52
  - CorrectPitch(), 21
  - repository, 21
- Ranadu package, 21
- rate of climb, 2, 15, 25
  - hydrostatic equation, 15
  - integrated acceleration, 15
  - Kalman filter, 36
  - memo, 36
  - new variable, 15
- reference frame, 6
  - a-frame, 5–8, 10, 11, 17, 18, 21–24, 32, 33, 38, 39
    - axes interchanged, 21
    - definition, 6
    - unit vectors, 6
  - aircraft, *see* reference frame, a-frame, 22
  - b-frame, 21
  - body, 21
  - Earth, *see* reference frame, l-frame
  - ENU, *see* reference frame, l-frame
  - inertial, 1, 6, 28

- inertialinertial, 22
- l-frame, 7, 8, 17, 18, 20–24, 30–33, 38, 39
  - motion of, 7
- l*-frame, 5, 6
- local-level, *see* reference frame, l-frame transformation, 5–8, 10, 11, 17, 18, 21–24, 30, 31, 33, 38
- repository
  - data used, 52
  - github, 21, 52
  - Ranadu, 21, 24
- reproducibility, 2, 52
- resolution
  - data recording, 29, 34, 36
- response
  - frequency, 3
- retrieval
  - measurements from IRU, 17
- ROC=rate of climb, 17, 36, 43, 44
- roll
  - correction
    - simplified, 21
- roll\*\*, 5, 6
- rotation rate of aircraft, 11, 29
  - a-frame, 11
  - measurement, 2, 5, 17
  - retrieved, 18
  - surrogate for measurement, 11, 18
- RStudio, 52, 53
- Schuler oscillation, 1, 20, 21, 30, 33, 34, 39, 47
  - period, 20
- script
  - processing, 2, 30
  - instructions, 2, 30
- sensitivity coefficient, *see* angle of attack, empirical representation
- separation
  - INS-GPS, 43, 47
- singularities, 28
- skew-symmetric, 17
- smoothing, 7, 20, 24, 30, 32, 34, 38–40
- spectral characteristics
  - high frequency, 36, 43
- spectrum
  - variance, 28, 34, 43–45, 47, 49
  - horizontal wind, 47, 49
  - rate of climb, 44
  - vertical wind, 45
- spline
  - cubic, 24
  - weight factors, 40
- standard deviation, *see* deviation, standard
- state transition matrix, *see* matrix, state transition
- state vector, 2–5, 7, 11, 28, 30, 33
  - definition, 1
  - derivative, 1–3, 5–7, 11, 14, 17, 18, 22, 27, 28, 30
  - extension, 27, 28
  - derivative function, 7
  - error in, 3
  - error-, *see* error-state vector
- static defect, 25
- strap-down inertial system, 22
- strong coupling, *see* coupling, strong supplement, 24, 52
- temperature, 15
- time lag, 7, 23, 24, 31
- time shift, 7
  - GPS vs. INS, 31
  - INS vs GPS, 31
- time step, 3, 27–29, 34
- timing
  - adjustment to, 36
- transformation
  - between reference frames, *see* reference frame, transformation
- transformation matrix
  - derivative, 5
- tuning, 28
- uncertainty
  - analysis for wind, 1
  - GPS-based measurements, 22, 27
  - reduction, 51
  - standard, 1
  - wind, 1

estimate, 1  
largest sources, 1  
technical note, 1

variable in data file  
  ACINS, 15, 43

variable in data files  
  AKRD, 43  
  ALT, 15, 34  
  ATTACK, 43  
  BLATA, 7  
  BNORMA, 7  
  BYAWR, 10  
  GGALT, 21  
  GGVEW, 21  
  GGVNS, 21  
  GGVSPD, 15, 43  
  LAT, 21  
  PITCH, 21  
  ROLL, 21  
  SSLIP, 43  
  TASX, 43  
  THDG, 21  
  VEW, 7, 21  
  VEWC, 43  
  VNS, 7, 21  
  VNSC, 43  
  VSPD, 7, 15

variable names  
  in R code, 3

variables  
  new from Kalman filter, 43  
  standard, *see* variable in data files

variables= in data files  
  BLONGA, 7

variance spectrum  
  noise, 28

velocity  
  derivative, 7

velocity of aircraft, 6, 7, 30  
  correction for GPS location, 29

derivative, 6, 8, 22

Earth-relative, 20

Kalman filter, 34, 36

I-frame, 18

velocity\*\*, 3, 5, 11, 34, 43  
vertical direction  
  local, 20

VSPD  
  characteristics, 36

wind  
  calculation, 43  
  Kalman-based, 43  
  standard, 47  
  corrected, Kalman filter, 2  
  horizontal  
    calculation, 36  
    uncertainty, 1  
  lateral, 47, 49  
  relative, 43  
  vertical  
    calculation, 15, 36  
    Kalman filter, 45  
    uncertainty, 1  
    variance spectrum, 43, 45  
    vertical\*\*, 1, 36, 43

wind\*\*, 1, 2, 43, 51

workflow document, 2, 6, 7, 17, 18, 21–24, 30, 52